CRITERION FOR THE PREVENTION OF CORE FRACTURE DURING EXTRUSION OF BIMETAL RODS

BY

Avitzur, B., Wu, R., Talbert, S., and Chou, Y. T.

Lehigh University
Institute for Metal Forming
Department of Metallurgy and Materials Engineering
Bethlehem, Pennsylvania 18015
September 1980

DISCLAIMER

TABLE OF CONTENTS

NOMENCLATURE

e	eccentricity factor
j^*	normalized total power consumption in extrusion
L/R_f	relative length of the bearing of the die
m	friction coefficient between the workpiece and the die
ml	coefficient of interface bonding strength
$r\%$	percent reduction in area
r_{fi}	the radial distance from the exit surface of the core deformation to the apex of the cone
r_{fs}	the radial distance from the exit surface of the sleeve deformation to the center of the toroid when it is independent of the angular position
r_{fs}^*	the radial distance from the exit surface of the sleeve deformation to the center of the toroid when it is a function of the angular position
r_{oi}	the radial distance from the entrance surface of the core deformation to the apex of the cone
r_{os}	the radial distance from the entrance surface of the sleeve deformation to the center of the toroid when it is independent of the angular position
r_{os}^*	the radial distance from the entrance surface of the sleeve deformation to the center of the toroid when it is a function of the angular position
R_f	the outer radius of the sleeve after forming
R_i	the interface radius between the core and the sleeve before forming
R_{fi}	the interface radius between the core and the sleeve after forming
R_i/R_o	relative core size
R_o	the outer radius of the sleeve before forming

$\dot{U}_{rc}$	velocity in r direction in the deformation zone of the core
$\dot{U}_{\theta c}$	velocity in θ direction in the deformation zone of the core
$\dot{U}_{\phi c}$	velocity in ϕ direction in the deformation zone of the core
$\dot{U}_{rs}$	velocity in r direction in the deformation zone of the sleeve
$\dot{U}_{\theta s}$	velocity in θ direction in the deformation zone of the sleeve
$\dot{U}_{\phi s}$	velocity in ϕ direction in the deformation zone of the sleeve
v_{fc}	outgoing velocity of the core
v_{fs}	outgoing velocity of the sleeve
v_o	incoming velocity of both the sleeve and core in extrusion
v_{oc}	incoming velocity of the core
v_{os}	incoming velocity of the sleeve
$\dot{W}_e$	the external power
$\dot{W}_f$	the friction loss along the bearing of the die
$\dot{W}_{fs}$	the friction loss between the sleeve and the die
$\dot{W}_{frc}$	the fracture energy associated with core fracture
$\dot{W}_{ic}$	the internal power of deformation in the core
$\dot{W}_{is}$	the internal power of deformation in the sleeve
$\dot{W}_{int}$	the shear power on the interface
$\dot{W}_{sc}$	the shear power in the core
$\dot{W}_{ss}$	the shear power in the sleeve
α	semicone angle of the die
α_i	semicone angle of the interface
ε	deviation factor
σ_{oc}	flow stress of the core
σ_{os}	flow stress of the sleeve
σ_{xf}	front pull stress
σ_{oc}/σ_{os}	relative flow stress of the core
σ_{os}/σ_{oc}	relative flow stress of the sleeve
σ_{xf}/σ_{oc}	relative forward tension

LIST OF FIGURES

CRITERION FOR THE PREVENTION OF CORE FRACTURE DURING EXTRUSION OF BIMETAL RODS

BY

Avitzur, B., Wu., R., Talbert, S., and Chou, Y.T.

ABSTRACT

Based on the upper-bound theorem in limit analysis, a theoretical model for core fracture in bimetal rods during extrusion has been developed and a fracture criterion established.

The variables affecting core fracture are: reduction in area (r%), die geometry, friction (m), relative size of the core and relative strength of the core. Within the wide range of possible combinations of these process variables, only a small range permits extrusion without fracture.

With suitable modifications the present analysis can be extended to develop criteria for sleeve fracture during extrusion and for both core and sleeve fracture during drawing.

1. INTRODUCTION

Bimetals are components composed of two separate metallic participants, each occupying a distinct position in the component. Bimetal (also called clad metal, duo- or dual-metal) rods or wires are made of two dissimilar metals. The core, a cylindrical body of one metal, is surrounded by a concentric, cylindrical sleeve of another metal. Some fibrous metals may also be regarded as bimetallic; for example, rods made by unidirectional solidification of some eutectic compositions contain a metallic (or nonmetallic) compound of fibrous filaments imbedded in an almost pure metallic matrix. The structure of present-day Nb-Sn superconducting wire is much more complex; it is multimetallic--containing more than two dissimilar metals.

The two elements of a bimetallic product are usually intimately interlocked in order to function in unison. The usefulness of bimetal rods or wire stems from the possibilities of combination of properties of dissimilar metals. For example:

1 Aluminum-clad steel wire combines the strength of steel with the electrical conductivity and corrosion resistivity of aluminum;

2 Superconductor core clad with copper sleeve combines superconductivity at cryogenic temperatures with assurance against failure when a local temporary rise in resistance or temperature occurs.

Although the number of desired combinations for practical use is virtually unlimited, the number of bimetallic combinations actually in use is limited, mainly because of manufacturing difficulties.

The object of this study is to define the forming conditions which will enable plastic deformation of a bimetal rod composed of two dissimilar metals to take place without core fracture. Although this fracture mode can be eliminated after a lengthy trial-and-error procedure in production lines, analysis of the problem could provide more economical solutions.

Numerous experimental studies of the production of bimetal rods are presented in Refs. 1-3. The analytical investigation of this problem has been done by Avitzur[4] and Osakada[5]. From their research, we may establish models based solely on the upper-bound approach and the concept of minimum energy, without any extraneous stress evaluation. These models describe the forming process of bimetal rods or wire by extrusion and drawing. Because of the complexity of the actual deformation patterns, separate models are used to simulate core and sleeve fracture in both extrusion and drawing respectively. At present, only the criterion for prevention of core fracture during extrusion has been derived. The criteria for the prevention of sleeve fracture during extrusion and for both core and sleeve fracture during drawing will be derived from similar velocity fields in the future.

These criteria can also be extended to the handling of failures such as fishskin and central burst (Refs. 6-11) in the mono-metal forming process, and for tube making.

Extrusion of a clad rod with a tight bond between the sleeve and the core is shown in Fig. 1.

As it passes through a die of semicone angle (α), the sleeve is forced to reduce in diameter from $2R_o$ to $2R_f$. At the same time, when sound flow occurs, the core is reduced proportionally from the diameter of $2R_i$ to $2R_{fi}$.

In co-extrusion, the following are the most common patterns of flow:

1. proportional flow with no fracture
2. defective flow with fracture of the core
3. defective flow with fracture of the sleeve.

These modes are shown in Figure 2.

As shown in Fig. 3, plastic flows of core and sleeve are modeled, respectively, by the spherical and the toroidal velocity fields. This aspect will be discussed in the derivation section.

The core and the sleeve must undergo indentical elongation for proportional flow to occur. The resulting deformation could be either homogeneous or nonhomogeneous. But for both situations, the following condition must prevail:

$$\frac{R_{fi}}{R_f} = \frac{R_i}{R_o} \tag{1}$$

where

R_o is the outer radius of the sleeve before forming,

R_i is the interface radius between the core and the sleeve before forming,

R_f is the outer radius of the sleeve after forming,

and R_{fi} is the interface radius between the core and the sleeve after forming.

When the core is harder than the sleeve it tends to undergo lower reduction than the sleeve. If the core undergoes less deformation than the sleeve, the core elongates less than the sleeve. Consequently, the sleeve exerts a tensile load on the core and, sooner or later, the core fractures. Mathematically, when the core fractures,

$$\frac{R_{fi}}{R_f} > \frac{R_i}{R_o} \tag{2}$$

When the sleeve is harder and undergoes less deformation than the core, the sleeve elongates less than the core. The core then pulls the sleeve to fracture it. Mathematically, when the sleeve fractures,

$$\frac{R_{fi}}{R_f} < \frac{R_i}{R_o} \tag{3}$$

Differential strengths of core and sleeve promote non-uniform flow leading to failure. Other factors, like interface bond as is studied through this manuscript, promote proportional flow and deter failure. The balance between these two driving forces determines the resulting mode of flow.

The failures in co-extrusion mentioned above, core fracture and sleeve fracture, result from the employment of improper combinations of the process variables, including percent reduction in area (r%), semicone angle of the die (α), the length of the bearing of the die (L/R_f), friction (m), coefficient of interface bonding strength (ml),

relative size of the core (R_i/R_o), relative strength and properties of the core (σ_{oc}/σ_{os}), and the prescribed body tractions, namely forward tension in extrusion (σ_{xf}/σ_{oc}).

Criterion for the prevention of core fracture during extrusion is found through the determination of the domains of the process variables wherein core fracture is expected. We use the upper-bound analysis to calculate the power expenditures involved in co-extrusion. For each particular combination of process variables, the power required for defective flow with core fracture and for proportional flow with sound product can be derived separately. The principle of minimum power states that for each combination of process parameters, the flow that consumes the least power will prevail for that particular combination of process variables. Following this principle, the boundary of the domain of core fracture is explicitly determined.

The criterion obtained through this method is presented in the result section. The related power calculation will also be described in the derivation section.

2. RESULTS

The criterion shown in Figs. 4(a,b&c) provides characteristic lines for the prevention of core fracture during extrusion. The abscissa is the ratio of the radius of the core to the radius of the sleeve (R_i/R_o) and the ordinate is the strength ratio of the sleeve to that of the core (σ_{os}/σ_{oc}). In each of these graphs core failure is expected on the shaded side of the curves. In all three figures, core fracture occurs only with intermediate-sized cores which are stronger than their sleeves, and is avoided with both smaller and larger sized cores. The varying parameters in Figs. 4a, b and c are semicone die angles (α), percent reduction in area (r%) and bond and friction levels (m and m1) respectively. In Figure 4a, the semicone angle of the die is the parameter, interface bond between the sleeve and core is perfect (m1 = 1), 30% reduction in area is effected, the coefficient of friction (m) is 0.05 and no back tension is applied. Below each characteristic line core fracture is expected, and above it core fracture is avoided. As shown, the higher the ratio σ_{oc}/σ_{os}, the larger is the fracture range for R_i/R_o; while for smaller die angles, the fracture zone is reduced. Figure 4b shows smaller core fracture regions for increasing reduction values. Figure 4c shows smaller core fracture regions for increasing friction and increasing interface bond strength.

The complexity of the characteristics expressed in Fig. 4 drives home the idea that it may be very hard to determine, without a rigorous analysis, the precise range of process variables where no core fracture

is expected. Trial and error experimental procedure may often fail or be prohibitively expensive. However, with the use of Eq. (17) derived later, curves like those in Fig. 4 can be constructed for any desired range of the parameters. The findings of this analysis are useful in further understanding the expected trends, and thus, may provide a guide in any experimental trial-and-error method.

Some general observations for the prevention of core fracture:

1. The harder the core, for $\sigma_{oc}/\sigma_{os} > 1$, the more likely it is that core fracture will occur, and the narrower becomes the range of process variables for a sound product.
2. The higher the mean pressure (higher back pressure, lower front tension), the wider the range of variables for which proportional flow is expected. Thus, in extrusion, the range of proportional flow is wider than in drawing.
3. Normally, the lower the friction ($\bar{m}$), the narrower the range for proportional flow in extrusion.
4. Larger percent reduction, smaller semicone angle and stronger interface bonding promotes the prevention of core fracture during extrusion.

3. DERIVATION

3.1 Foreword

First, two separate, kinematically admissible velocity fields are introduced for the core and sleeve respectively. Strain rates for the corresponding fields and power consumption of the process are then derived. Finally, the characteristics of the power consumption in the domain of two pseudoindependent process parameters is disussed.

3.2 Velocity Fields

3.2.1 General The flow of the core material and that of the sleeve material are considered separately with matching boundary conditions. The spherical velocity field is chosen to describe the deformation of the core. The toroidal velocity field simulates the deformation of the sleeve.

3.2.2 Core (Spherical Field) The spherical field is described in Ref. 12, Sec. 8.3, as follows:

> "A kinematically admissible velocity field is described in Fig. 5. The rod is divided into three regions in which the velocity field is continuous. In zone Ic and IIIc the velocity is uniform and has an axial component only. In zone Ic the velocity is v_{oc}, and in zone IIIc the velocity is v_{fc}. Because of volume constancy

$$v_{oc} = v_{fc} \left(R_{fi}/R_i\right)^2 \tag{4}$$

In zone Ic deformation has not yet begun. It includes the incoming rod, which is separated from the deforming zone IIc by the surface Γ_{2c}. Surface Γ_{2c} is spherical, of radius r_{oi} with the origin at the apex 0 of the cone of the angle α_i. Zone IIc is the zone of deformation bounded by the surface of the cone with a cone of an included angle $2\alpha_i$ and two concentric spherical surfaces Γ_{1c} and Γ_{2c}. The surface Γ_{2c} is the previously mentioned spherical boundary between zones Ic and IIc. The spherical surface Γ_{1c} of radius r_{fi} with the origin at the apex 0 of the cone, separates zone IIc from the emerging product of zone IIIc. In zone IIc the velocity is directed toward the apex 0 of the cone, with cylindrical symmetry.

"In the spherical coordinate system (r,θ,ϕ), the velocity components for zone IIc are

$$\left.\begin{aligned} \dot{U}_{rc} &= -v_{oc}\frac{r_{oi}^2}{r^2}\cos\theta \\ \dot{U}_{\theta c} &= \dot{U}_{\phi c} = 0 \end{aligned}\right\} \qquad (5)$$

Across the boundaries Γ_{1c} and Γ_{2c}, the components of velocity normal to the surfaces (Γ_{1c} and Γ_{2c}) are continuous. There exist velocity discontinuities parallel to these surfaces."

3.2.3 Sleeve (Toroidal Field)

Figure 6 shows the velocity field of the sleeve. Similar to that in the core, there are rigid flow zones I_s and III_s and the deformation zone II_s.

In zone II_s the toroidal coordinate system is used. The circle (0') at the distance e from the axis of symmetry is an origin. This e will be named as 'eccentricity factor' from here on. The radial distance from 0' is r, varying from r_{fs}^* on Γ_{1s} to r_{os}^* on Γ_{2s} (r_{fs}^* and r_{os}^* can be functions of the angular position; they will be determined later). The angular position θ varies from α_i (by Eq. (8)) on the inner conical surface Γ_{cs} to α on the conical surface of the die Γ_{3s}. Please note that $\alpha_i > 0$. The direction of θ is normal to the direction of r. Normal to these two axes (r and θ) is the ϕ-axis. Axial symmetry exists with respect to ϕ.

In this toroidal coordinate system, the velocity is assumed to obey

$$\left.\begin{aligned} \dot{U}_{rs} &= -v_{os}\,\frac{\dot{r}_{os}^*\,(r_{os}^* \sin\theta + c)}{r\,(r\sin\theta + e)}\,\cos\theta \\ \dot{U}_{\theta s} &= \dot{U}_{\phi s} = 0 \end{aligned}\right\} \qquad (6)$$

where r_{os}^* is the radial distance between Γ_{2s} and 0'

r_{fs}^* is the radial distance between Γ_{1s} and 0'

It is noted here that the deformation zone II_s is bounded by surfaces Γ_{3s}, Γ_{2s}, Γ_{cs} and Γ_{1s}. Γ_{3s} is the outer conical surface of the sleeve and is predetermined by the semicone angle of the die α. For simplicity, the surface of discontinuity Γ_{2s} is assumed to be a toroidal surface.

The radial distance r_{os}^* of this surface from the toroidal center 0' depends only on the eccentricity factor e. Mathematically, this means

$$r_{os}^* = r_{os} = \frac{R_o - e}{\sin\alpha} , \tag{7}$$

which is independent of the angular position θ. The inner conical surface of the sleeve Γ_{cs} is also determined through the value of the eccentricity factor e. The semicone angle α_i of the surface Γ_{cs} is thus a function of e. From the proposed geometry of Fig. 6, we found that

$$\alpha_i = \sin^{-1}\left\{\frac{R_i - e}{R_o - e}\sin\alpha\right\} \tag{8}$$

The value of e itself is pseudoindependent, namely, the value is arbitrary during the evaluation of the strains and power consumptions and is, finally, determined by the concept of minimum energy. (See Ref. 13 for detailed discussion on "limit analysis," the "upper bound approach" and the concept of minimum energy.)

In Fig. 7a a special case of proportional deformation, namely, homogeneous deformation with a spherical flow (e=0) , is described. Even when $e \neq 0$ and a toroidal flow exists (see Fig. 7b), it still may be proportional, so that R_{fi} is determined through Eq. (1) and is not a function of the eccentricity (e). Under this circumstance, the surface Γ_{2s} is toroidal (by our choice) and the angle α_i is defined by Eq. (8). The surface Γ_{1s} is not toroidal (if $e \neq 0$) and is determined subsequently.

In order to render the exit inner radius R_{fi} a variable and permit the flow to become nonproportional, the deviation factor ε was introduced as a second pseudoindependent parameter. Both the inner radius R_{fi} and the surface Γ_{ls} are then functions of ε and also of e. Since the introduction of the deviation factor ε will introduce thinning or thickening of the emerging sleeve, it will also introduce a change in the ratio of exit to incoming sleeve velocity.

From the established geometry, it is found that the relationship between the incoming velocity v_{os} of the rigid zone I_s and the exit velocity v_{fs} of the outgoing rigid zone III_s depends on pseudoindependent parameters e and ε. We define this relationship as

$$\frac{v_{os}}{v_{fs}} \equiv \left(\frac{R_f}{R_o}\right)^2 \left(1 - 2\varepsilon \frac{e}{R_o}\right) \tag{9}$$

Whenever e or ε is equal to zero, this relationship dictates the proportional flow condition. For nonzero e and ε the variations in R_{fi} and the surface Γ_{ls} are illustrated in Fig. 7c. In this figure, when $e\varepsilon > 0$ the ratio of exit velocity to entrance velocity will be larger than that for the proportional flow [according to Eq. (9)]. This will lead to the thinning of the sleeve. The surface Γ_{ls} thus moves to the left side of the proportional position (which is designated as Γ_{ls}'); R_{fi}, therefore, increases to R_{fi}'. When $e\varepsilon < 0$, changes of Γ_{ls} and R_{fi} will be reversed. They are shown as Γ_{ls}'' and R_{fi}'' in Fig. 7c.

Based on volume constancy and the defined velocity field, the radial distance r_{fs}^* of Γ_{ls} from $0'$ as obtained in the Appendix is:

$$r_{fs}^*(\theta,e,\varepsilon) = -\frac{e}{\sin\theta} + \frac{R_o}{\sin\theta}\sqrt{\frac{v_{os}}{v_{fs}}\left[\left\langle\frac{\sin\theta}{\sin\alpha} + \frac{e}{R_o}\left(1 - \frac{\sin\theta}{\sin\alpha}\right)\right\rangle^2 - 1\right] + \left(\frac{R_f}{R_o}\right)^2} \qquad (10$$

where the ratio v_{os}/v_{fs} is defined by Eq. (9).
The dimension of R_{fi} is, therefore, found to be

$$R_{fi} = [(r_{fs}^*)_{\theta=\alpha_i} \sin\alpha_i + e]$$

$$= R_o\left\{\frac{v_{os}}{v_{fs}}\left[\left\langle\frac{\sin\alpha_i}{\sin\alpha} + \frac{e}{R_o}\left(1 - \frac{\sin\alpha_i}{\sin\alpha}\right)\right\rangle^2 - 1\right] + \left(\frac{R_f}{R_o}\right)^2\right\}^{\frac{1}{2}} \qquad (11)$$

3.3 Strain Rates

In upper-bound analysis, the power to overcome the resistance of the material to deformation is estimated through the integration of the function which contains the strain rate and the yield stress over the entire deformation volume. Therefore, it is necessary to derive the strain rates for the proposed spherical and toroidal fields.

The strain rates in the spherical field as functions of velocity components are (Ref. 14):

$$\left.\begin{aligned}
\dot{\varepsilon}_{rr} &= \frac{\partial\dot{U}_r}{\partial r} \qquad \dot{\varepsilon}_{\theta\theta} = \frac{1}{r}\frac{\partial\dot{U}_\theta}{\partial\theta} + \frac{\dot{U}_r}{r} \\
\dot{\varepsilon}_{\phi\phi} &= \frac{1}{r\sin\theta}\frac{\partial\dot{U}_\phi}{\partial\phi} + \frac{\dot{U}_r}{r} + \frac{\dot{U}_\theta}{r}\cot\theta \\
\dot{\varepsilon}_{r\theta} &= \frac{1}{2}\left(\frac{\partial\dot{U}_\theta}{\partial r} - \frac{\dot{U}_\theta}{r} + \frac{1}{r}\frac{\partial\dot{U}_r}{\partial\theta}\right) \\
\dot{\varepsilon}_{\theta\phi} &= \frac{1}{2}\left(\frac{1}{r\sin\theta}\frac{\partial\dot{U}_\theta}{\partial\phi} + \frac{1}{r}\frac{\partial\dot{U}_\phi}{\partial\theta} - \frac{\cot\theta}{r}\dot{U}_\phi\right) \\
\dot{\varepsilon}_{\phi r} &= \frac{1}{2}\left(\frac{\partial\dot{U}_\phi}{\partial r} - \frac{\dot{U}_\phi}{r} + \frac{1}{r\sin\theta}\frac{\partial\dot{U}_r}{\partial\phi}\right)
\end{aligned}\right\} \qquad (12)$$

According to Sokolnikoff (Eqs. 48.7 and 48.9 of Ref. 15) the strain rates are:

$$\left.\begin{aligned} \dot{\varepsilon}_{ii} &= \frac{\partial}{\partial \alpha_i}\frac{\dot{U}_i}{\sqrt{g_{ii}}} + \frac{1}{2g_{ii}}\sum_{k=1}^{3}\frac{\partial g_{ii}}{\partial \alpha_k}\frac{\dot{U}_k}{\sqrt{g_{kk}}} \qquad \text{if } i = j \\ \dot{\varepsilon}_{ij} &= \frac{1}{2\sqrt{g_{ii}g_{jj}}}\left[g_{ii}\frac{\partial}{\partial \alpha_j}\left(\frac{\dot{U}_i}{\sqrt{g_{ii}}}\right) + g_{jj}\frac{\partial}{\partial \alpha_i}\left(\frac{\dot{U}_j}{\sqrt{g_{jj}}}\right)\right] \text{ if } i \neq j \end{aligned}\right\} \quad (13)$$

where

$$g_{rr} = 1, \quad g_{\theta\theta} = r^2 \quad \text{and} \quad g_{\phi\phi} = (r\sin\theta + e)^2$$

for the present toroidal field.

Calculating the strain rates, substituting $\dot{U}_\theta = \dot{U}\phi = o$,

$$\left.\begin{aligned} \dot{\varepsilon}_{rr} &= \frac{\partial \dot{U}_r}{\partial r} \\ \dot{\varepsilon}_{\theta\theta} &= \frac{\dot{U}_r}{r} \\ \dot{\varepsilon}_{\phi\phi} &= \frac{\dot{U}_r \sin\theta}{r\sin\theta + e} \\ \dot{\varepsilon}_{r\theta} &= \frac{1}{2r}\frac{\partial \dot{U}_r}{\partial \theta} \\ \dot{\varepsilon}_{\theta\phi} &= \dot{\varepsilon}_{r\phi} = o \end{aligned}\right\} \quad (14)$$

From Eqs. (5) and (12), the strain rates for the spherical field can be calculated. They are

$$\left.\begin{aligned} \dot{\varepsilon}_{rr} &= -2\dot{\varepsilon}_{\theta\theta} = -2\dot{\varepsilon}_{\phi\phi} = 2\,V_{oc}r_{oi}^2\frac{\cos\theta}{r^3} \\ \dot{\varepsilon}_{r\theta} &= \frac{1}{2}V_{oc}r_{oi}^2\frac{\sin\theta}{r^3} \\ \dot{\varepsilon}_{\theta\phi} &= \dot{\varepsilon}_{r\phi} = o \end{aligned}\right\} \quad (15)$$

Similarly, Eqs. (6) and (14) give us the strain rates for toroidal field:

$$\left.\begin{aligned}
\dot{\varepsilon}_{rr} &= V_{os}\ \frac{r_{os}\,(r_{os}\sin\theta + e)(2\,r\sin\theta + e)}{r^2\,(r\sin\theta + e)^2}\cos\theta \\
\dot{\varepsilon}_{\theta\theta} &= -V_{os}\ \frac{r_{os}\,(r_{os}\sin\theta + e)}{r^2(r\sin\theta + e)}\cos\theta \\
\dot{\varepsilon}_{\phi\phi} &= -V_{os}\ \frac{r_{os}\,(r_{os}\sin\theta + e)}{r\,(r\sin\theta + e)^2}\sin\theta\cos\theta \\
\dot{\varepsilon}_{r\theta} &= \frac{1}{2}\,V_{os}\ \frac{r_{os}\,[r\sin\theta + e)(r_{os}\sin\theta + e)\sin\theta - e(r_{os}-r)\cos^2\theta]}{r^2\,(r\sin\theta + e)^2} \\
\dot{\varepsilon}_{\theta\phi} &= \dot{\varepsilon}_{r\phi} = 0
\end{aligned}\right\} \qquad (16)$$

The compressibility equation $\dot{\varepsilon}_{rr} + \dot{\varepsilon}_{\theta\theta} + \dot{\varepsilon}_{\phi\phi} = 0$ is held for the above expressions.

3.4 Normalized Total Power Consumption (j*)

3.4.1 General

The upper bound on power consumption during co-extrusion sleeve and core composed of two dissimilar materials is given by

$$j^* = (\dot{W}_e + \dot{W}_{ic} + \dot{W}_{sc} + \dot{W}_f + \dot{W}_{is} + \dot{W}_{int} + \dot{W}_{ss} + \dot{W}_{fs} + \dot{W}_{frc}) \,/\, \pi\sigma_{oc} v_o R_o^2 \qquad (17)$$

where, for extrusion $v_o = v_{os} = v_{oc}$.

The definitions of the individual power terms follow.

3.4.2 The External Power: $\dot{W}_e$

The external power $\dot{W}_e$ is associated with the prescribed surface tractions. For extrusion, the prescribed surface traction is the front tension σ_{xf}, and the external power becomes

$$\dot{W}_e = \dot{W}_f = \pi \left\{ v_{fc} R_{fi}^2 + v_{fs}(R_f^2 - R_{fi}^2) \right\} \sigma_{xf} \qquad (18)$$

3.4.3 The Internal Power of Deformation in the Core: $\dot{W}_{ic}$

For the core, the simple spherical field of Eq. (5) was assumed through this entire work. With this spherical field, the internal power of deformation in the core, by Eq. (8.11) of Ref. 12, becomes

$$\dot{W}_{ic} = \frac{2}{\sqrt{3}} \sigma_{oc} \int_{o}^{\alpha_i} \int_{r_{fi}}^{r_{oi}} v_{oc} r_{oi}^{2} \frac{1}{r^3} \sqrt{3\cos^2\theta + \frac{1}{4}\sin^2\theta}\, (2\pi r \sin\theta\, r\, dr\, d\theta)$$

$$= 2\pi\sigma_{oc} v_{oc} R_i^{2} f(\alpha_i) \ln(R_i/R_{fi}) \qquad (19)$$

where $f(\theta)$ is defined by

$$f(\theta) = \frac{1}{\sin^2\theta} \left[1 - \cos\theta \sqrt{1 - \frac{11}{12}\sin^2\theta} + \frac{1}{\sqrt{11 \cdot 12}} \ln \frac{1 + \sqrt{\frac{11}{12}}}{\sqrt{\frac{11}{12}}\cos\theta + \sqrt{1 - \frac{11}{12}\sin^2\theta}} \right] \qquad (20)$$

The function $f(\theta)$ is tabulated in Table 8.1 of Ref. 12, for 1° intervals for $0 \leq \theta \leq 90°$. Table 8.1 of Ref. 12 is reproduced here as Table 1. Please note that $f(\theta)$ is within 5% error if replaced by 1 for θ up to 67°.

Table 1 Relative Average Effective Strain $f(\alpha)$ and Shear Losses

$\alpha°$	$f(\alpha)$	$\frac{\alpha}{\sin^2\alpha} - \cot\alpha$	$\alpha°$	$f(\alpha)$	$\frac{\alpha}{\sin^2\alpha} - \cot\alpha$	$\alpha°$	$f(\alpha)$	$\frac{\alpha}{\sin^2\alpha} - \cot\alpha$
0	1.00000	0						
1	1.00001	0.011636	31	1.00672	0.37539	61	1.03603	0.83746
2	1.00003	0.023275	32	1.00721	0.38854	62	1.03784	0.85632
3	1.00006	0.034920	33	1.00772	0.40180	63	1.03974	0.87549
4	1.00010	0.046573	34	1.00825	0.41516	64	1.04174	0.89500
5	1.00016	0.058237	35	1.00881	0.42864	65	1.04384	0.91484
6	1.00023	0.069915	36	1.00939	0.44224	66	1.04605	0.93503
7	1.00031	0.081611	37	1.01000	0.45596	67	1.04838	0.95559
8	1.00041	0.093327	38	1.01063	0.46981	68	1.05082	0.97653
9	1.00052	0.10507	39	1.01129	0.48380	69	1.05340	0.99787
10	1.00064	0.11683	40	1.01198	0.49792	70	1.05613	1.01961
11	1.00078	0.12862	41	1.01270	0.51218	71	1.05900	1.04178
12	1.00093	0.14045	42	1.01345	0.52660	72	1.06204	1.06438
13	1.00109	0.15231	43	1.01423	0.54117	73	1.06526	1.08745
14	1.00127	0.16421	44	1.01505	0.55590	74	1.06867	1.11099
15	1.00146	0.17614	45	1.01590	0.57080	75	1.07228	1.13503
16	1.00167	0.18813	46	1.01679	0.58587	76	1.07611	1.15958
17	1.00189	0.20016	47	1.01772	0.60111	77	1.08018	1.18467
18	1.00212	0.21223	48	1.01869	0.61655	78	1.08451	1.21031
19	1.00237	0.22437	49	1.01970	0.63217	79	1.08912	1.23653
20	1.00264	0.23656	50	1.02075	0.64800	80	1.09404	1.26335
21	1.00292	0.24881	51	1.02185	0.66403	81	1.09928	1.29080
22	1.00322	0.26112	52	1.02300	0.68027	82	1.10488	1.31890
23	1.00354	0.27350	53	1.02420	0.69674	83	1.11087	1.34768
24	1.00387	0.28595	54	1.02546	0.71344	84	1.11727	1.37717
25	1.00422	0.29848	55	1.02677	0.73037	85	1.12413	1.40740
26	1.00459	0.31108	56	1.02814	0.74755	86	1.13148	1.43840
27	1.00498	0.32377	57	1.02958	0.76498	87	1.13935	1.47020
28	1.00538	0.33653	58	1.03108	0.78268	88	1.14780	1.50284
29	1.00581	0.34939	59	1.03265	0.80066	89	1.15687	1.53636
30	1.00625	0.36234	60	1.03430	0.81891	90	1.16660	1.57080

3.4.4 The Shear Power in the Core: $\dot{W}_{sc}$

The shear power over surfaces of velocity discontinuity Γ_{2c} by Eq. (8.12) of Ref. 12, becomes

$$\left.\begin{aligned}\dot{W}_{sc} &= \frac{1}{\sqrt{3}}\,\sigma_{oc}\int_0^{\alpha_i} v_{oc}\,\sin\theta\,(2\pi r_{oi}\,\sin\theta\,r_{oi}\,d\theta)\\ &= \frac{1}{\sqrt{3}}\,\pi\sigma_{oc}\,v_{oc}\,R_i^{\,2}\left(\frac{\alpha_i}{\sin^2\alpha_i} - \cot\alpha_i\right)\end{aligned}\right\} \qquad (21)$$

3.4.5 The Friction Loss along the Bearing of the Die: $\dot{W}_f$

The friction power losses between the sleeve and the cylindrical portion of the die (bearing of the die) are independent of the assumed velocity field. They are

$$\dot{W}_f = \frac{2}{\sqrt{3}}\,m\pi\sigma_{os}\,v_{fx}\,R_f^{\,2}\left(\frac{L}{R_f}\right) \qquad (22)$$

3.4.6 The Internal Power of Deformation in the Sleeve: $\dot{W}_{is}$

The internal power of deformation in the sleeve $\dot{W}_{is}$, by the toroidal field, is obtained as follows:

$$\dot{W}_{is} = \frac{2}{\sqrt{3}}\,\sigma_{os}\int_{\alpha_i}^{\alpha}\int_{r_{fs}^*}^{r_{os}}\sqrt{\frac{1}{2}\,\dot{\varepsilon}_{ij}\dot{\varepsilon}_{ij}}\;2\pi(r\sin\theta + e)\,r\,d\theta\,dr \qquad (23)$$

where $$\frac{1}{2}\,\dot{\varepsilon}_{ij}\dot{\varepsilon}_{ij} = \frac{1}{2}\,(\dot{\varepsilon}_{rr}^{\,2} + \dot{\varepsilon}_{\theta\theta}^{\,2} + \dot{\varepsilon}_{\phi\phi}^{\,2}) + \dot{\varepsilon}_{r\theta}^{\,2} \qquad (24)$$

[$\dot{\varepsilon}_{rr}$, $\dot{\varepsilon}_{\theta\theta}$, $\dot{\varepsilon}_{\phi\phi}$ and $\dot{\varepsilon}_{r\theta}$ were calculated and listed in Eqs. (16).]

α_i is defined by Eq. (8)

r_{fs}^* is defined by Eq. (10)

r_{os} is defined by Eq. (7)

3.4.7 The Shear Power on the Interface : $\dot{W}_{int}$

The shear loss over the conical interface between the core and the sleeve is due to the discontinuity in the tangential components of the assumed velocity fields. Because the normal component is zero, the equation for the shear loss is

$$\dot{W}_{int} = \int_{\Gamma_{cs}} m_1 \Gamma \left| \dot{U}_{rs} - \dot{U}_{rc} \right| ds \qquad (25)$$

where m_1 is the coefficient describing the bonding condition, $0 \leq m_1 \leq 1$,

Γ_{cs} is the conical surface of separation,

and Γ is the lower of the two ratios,

$$\frac{\sigma_{os}}{\sqrt{3}} \text{ and } \frac{\sigma_{oc}}{\sqrt{3}} .$$

Consequently, algebraic complications are avoided if the equivalent equation

$$\dot{W}_{int} = m_1 \left| \int_{\Gamma_{cs}} \Gamma \dot{U}_{rs} ds - \int_{\Gamma_{cs}} \Gamma \dot{U}_{rc} ds \right| \qquad (26)$$

is used where the integrals are computed separately with different variables.

In the first integral,

$$ds = 2\pi (r \sin\alpha_i + e)\, dr \qquad (27)$$

$$\dot{U}_{rs} = -V_{os} \frac{r_{os}}{r} \left(\frac{r_{os} \sin\alpha_i + e}{r \sin\alpha_i + e} \right) \cos\alpha_i \qquad (28)$$

and the limits of the integration are

$$\frac{R_{fi} - e}{\sin\alpha_i} \leq r \leq \frac{R_i - e}{\sin\alpha_i} \qquad (29)$$

In the second integral,

$$ds = 2\pi r \sin\alpha_i\, dr \qquad (30)$$

$$\dot{U}_{rc} = -V_{oc} \frac{R_i^2 \cos\alpha_i}{r^2 \sin^2\alpha_i} \qquad (31)$$

and

$$\frac{R_{fi}}{\sin\alpha_i} \leq r \leq \frac{R_i}{\sin\alpha_i} \qquad (32)$$

The result of this shear loss computation then becomes

$$\dot{W}_{int} = \frac{2\pi}{\sqrt{3}} m\dot{l} \cdot \min\left[\sigma_{oc}, \sigma_{os}\right] \cdot V_o$$

$$\cdot \left| \left\{ R_i (R_i - e) \cot\alpha_i \ln \frac{R_i - e}{R_{fi} - e} - R_i^2 \cot\alpha_i \ln \frac{R_i}{R_{fi}} \right\} \right| \quad (33)$$

where $\min [\sigma_{oc}, \sigma_{os}]$ is the smaller of σ_{oc} and σ_{os}.

3.4.8 The Shear Power in the Sleeve : $\dot{W}_{ss}$

The shear power on the surfaces of velocity discontinuity Γ_{1s} and Γ_{2s} is given by the following two equations:

$$\dot{W}_{\Gamma_{2s}} = \frac{\sigma_{os}}{\sqrt{3}} \int_{\Gamma_{2s}} V_o \sin\theta \, ds$$

$$= \frac{\sigma_{os}}{\sqrt{3}} \int_{\alpha_i}^{\alpha} (V_o \sin\theta) \cdot 2\pi (r_o \sin\theta + e) r_o d\theta \quad (34)$$

and $$\dot{W}_{\Gamma_{1s}} = \frac{\sigma_{os}}{\sqrt{3}} \int_{\Gamma_{1s}} \left| V_{fs} \sin(\theta - \psi) + \left(- \dot{U}_{rs} \right)_{r=r_{fs}^*} \sin\psi \right| ds$$

$$= \frac{\sigma_{os}}{\sqrt{3}} \int_{\alpha_i}^{\alpha} \left| V_{fs} \sin(\theta - \psi) + V_{os} \frac{r_{os}(r_{os}\sin\theta + e)}{r_{fs}^*(r_{fs}^* \sin\theta + e)} \cos\theta \sin\psi \right| \cdot 2\pi (r_{fs}^* \sin\theta + e) r_{fs}^* d\theta \quad (35)$$

where ψ is the angle between the plane normal to the surface Γ_{1s} and the radial direction of the toroidal coordinate, i.e.,

$$\psi = \tan^{-1} \left\{ \frac{1}{r_{fs}^*} \cdot \frac{d r_{fs}^*}{d\theta} \right\} \quad (36)$$

The total shear loss in the sleeve is therefore

$$\dot{W}_{ss} = \dot{W}_{\Gamma_{2s}} + \dot{W}_{\Gamma_{1s}} \quad (37)$$

3.4.9 The Friction Loss Between the Sleeve and the Surface of the Die: $\dot{W}_{fs}$

This friction loss is calculated by

$$\dot{W}_{fs} = \frac{\sigma_{os}}{\sqrt{3}} m \int_{(r_{fs}^*)_{\theta=\alpha}}^{r_{os}} \left|(\dot{U}_{rs})_{\theta=\alpha}\right| 2\pi (r\sin\alpha + e)\, dr \tag{38}$$

3.4.10 The Fracture Energy Associated with Core Fracture: $\dot{W}_{frc}$

If core fracture occurs, there must have been volume separation along Γ_{lc}. That is, velocity discontinuity appears in the directions of both the plane normal and the tangent of the Γ_{lc} surface. The energy consumption associated with this event as given by Eq. (57c) of Ref. 13 is,

$$\dot{W}_{frc} = \sigma_{oc} \int_{\Gamma} \sqrt{\frac{(\Delta v_T)^2}{3} + \Delta v_N^2}\, ds \tag{39}$$

where

$$\Delta v_N = v_{fs} \cos\theta - v_{oc} \left(\frac{r_{oi}}{r_{fi}}\right)^2 \cos\theta \tag{40}$$

$$\Delta v_T = v_{fs} \sin\theta \tag{41}$$

$$ds = 2\pi (r_{fi} \sin\theta)\, r_{fi} d\theta \tag{42}$$

3.5 The Characteristics of j*; The Contour Lines

The individual power terms of Eqs. (23), (34), (35), (38) and (39) are presented in integral form. Precise analytical integration of these terms was not performed. Before further analysis and approximations are made, it is helpful to analyze the characteristics of the total power j*.

These characteristics are studied by performing numerical integration. Specifically, the effect of the two pseudoindependent parameters, namely, the eccentricity factor (e/R_o) and the deviation factor (ε) on the total power j^* is presented in the form of j^* contour lines.

Each specific combination of process variables is associated with a set of j^* contour lines in the e/R_o and ε domain. The extrusion process begins with homogeneous proportional flow, which means e/R_o and ε are originally zero. As deformation proceeds, the process chooses the flow pattern that minimizes the j^* without the addition of extrusion power. Therefore, the location of the minimum j^* determines the type of flow - proportional flow or defective flow with core fracture - that takes place.

By examining Eq. (9) we know that core fracture is associated with $e\varepsilon > 0$, and $e\varepsilon = 0$ defines proportional flow. Four different types of j^* contour lines are given in Figs. 8 - 11 . The conditions in each of Figs. 8 - 11 are identified by the respective stars on Fig. 4a . In Fig. 8 , the origin is a global minimum, while it is a local minimum in Fig. 9a . Figure 9b is the enlarged portion of Fig. 9a in the vicinity of the origin. Figure 10 shows that the minimum is on the e/R_o axis. In Figs. 8 - 10 the minimum value of j^* is at $e\varepsilon = 0$. Proportional flow is expected in those situations. Figure 11 is an example of core fracture with $e\varepsilon > 0$.

4. THE CONSTRUCTION OF FRACTURE CRITERION CURVES

As observed in the earlier section and in Eqs. (5) and (6), proportional flow is expected when the minimum value of j^* exists anywhere along the axis of Figs. 8-10; namely, along $e = 0$ or $\varepsilon = 0$, including the origin where $e = \varepsilon = 0$. Core fracture will occur when

$$\left.\frac{\partial j^*}{\partial e}\right|_{\substack{\varepsilon=0 \\ e=0}} < 0 \qquad \text{and} \qquad \left.\frac{\partial j^*}{\partial \varepsilon}\right|_{\substack{e>0 \\ \varepsilon=0}} < 0 \tag{43}$$

The first of Eqs. (43) suggests that one condition necessary for the occurrence of core fracture is that the slope of j^* at $\varepsilon = 0$ (along the e axis) will lead away from the origin, at a positive e value. This condition, although necessary, is not in itself sufficient to cause such fracture. For example, the processing conditions handled in Fig. 10 lead to a minimum of j^* along the e axis at $e/R_o = 0.24$. The flow, nevertheless, is proportional and fracture does not occur. The power required is lower than that required for a homogeneous flow by the spherical field for $e = \varepsilon = 0$.

The observation suggests that a combined spherical/toroidal field for a homogeneous material may provide a lower upper-bound than will the conventional spherical field.[12] However, since the complexity of the solution might not justify the improvement, the present study will not concern itself with that aspect.

The second requirement that supplements the first of Eqs. (43) is that when the first condition is satisfied, the slope of j^* with respect

to ε (for positive ε) for any positive value of e will also be negative. Note that along the ε axis, when e = 0, the slope of j* with respect to ε is automatically zero.

Numerically, the two necessary conditions of Eqs. (43) can be evaluated from Eq. (17) as follows:

$$\frac{j^*(\varepsilon=0,\ e) - j^*(\varepsilon=0,\ e=0)}{e} < 0$$

$$\frac{j^*(\varepsilon,\ e_1) - j^*(\varepsilon=0,\ e_1)}{\varepsilon} < 0 \qquad (44)$$

where $e \ll 1,\ e_1 \ll 1,\ \varepsilon \ll 1$

In evaluating the slopes of Eqs. (44) it is helpful to note that j* at the point $e = \varepsilon = 0$ is determined analytically through the following solution;

$$j^*(e=0,\ \varepsilon=0) = \frac{\sigma_{xf}}{\sigma_{oc}} + 2\left(\frac{R_i}{R_o}\right)^2 f(\alpha_{ih})\ \ell n\frac{R_o}{R_f} + \frac{2}{\sqrt{3}}\left(\frac{R_i}{R_o}\right)^2 \left(\frac{\alpha_{ih}}{\sin^2\alpha_{ih}} - \cot\alpha_{ih}\right)$$

$$+ 2\,\frac{\sigma_{os}}{\sigma_{oc}}\left[f(\alpha) - \left(\frac{R_i}{R_o}\right)^2 f(\alpha_{ih})\right] \ell n\frac{R_o}{R_f}$$

$$+ \frac{2}{\sqrt{3}}\,\frac{\sigma_{os}}{\sigma_{oc}}\left[\frac{\alpha}{\sin^2\alpha} - \cot\alpha - \left(\frac{\alpha_{ih}}{\sin^2\alpha_{ih}} - \cot\alpha_{ih}\right)\right]$$

$$+ \frac{2}{\sqrt{3}}\,m\,\frac{\sigma_{os}}{\sigma_{oc}}\cot\alpha\ \ell n\frac{R_o}{R_f} \qquad (45)$$

where $\alpha_{ih} = \sin^{-1}\left\{\frac{R_i}{R_o}\sin\alpha\right\}$

The above equation is easily obtained using Eq. (8-16b) and (8-17b) of Ref. 12 for the calculation of forces. For the core, α is replaced by α_i. For the sleeve, the solution for $\alpha=\alpha_i$ is subtracted from the same solution with α.

Figures 4 were constructed by the substitution of the values from Eq. 17 for j^* into Eqs. (44). The solid lines define the border between positive and negative slopes for the first of Eqs. (44); the dashed lines for the second. The above numerical integration and differentiation are time-consuming processes and require larger computers.

The present results suggest that an attempt should be made to perform the integration of Eq. (17) and the differentiation of Eqs. (43) only in the immediate proximity of the origin, for $e \ll 1$ and $\varepsilon \ll 1$. When these expressions are determined, Figs. 4 and figures like them will be constructed from explicit expressions at a fraction of the cost of the present runs.

REFERENCES

1 Matsuura, Y., and Takase, K., "An Experimental Study and the Solution of Energy Method on Plastic Deformation of Two-Phase Combination Materials Consisting of Copper and Aluminum," J. of Japan Society for Technology of Plasticity, Vol. 15, No. 157, (1974-2)

2 Avitzur, B., Zoerner, W., and Austen, A., "Hydrostatic Extrusion of Hard Core Clad Rod," J. of Basic Eng., ASME Trans., March 1972, 78-80.

3 Avitzur, B., Story, J.M., and Hahn, W.C., "The Effect of Receiver Pressure on the Observed Flow Pattern in the Hydrostatic Extrusion of Bi-Metal Rods," J. of Eng. for Industry, Aug. 1976, 909-913.

4 Avitzur, B., "The Production of Bi-Metal Rod and Wire," The Wire J., Vol. 3, No. 8, Aug. 1970, pp. 42-49.

5 Osakada, K., Limb, M., and Mellor, P.B., "Hydrostatic Extrusion of Composite Rods with Hard Cores," Int. J. Mech. Sci., Pergamon Press, Vol. 15, 1973, pp. 291-307.

6 Jennison, H.C., "Certain Types of Defects in Copper Wire Caused by Improper Dies and Drawing Practice," Technical Publication No. 285, Class E, Institute of Metals, No. 97, The American Institute of Mining and Metallurgical Engineers, 1930.

7 Orbegozo, J.I., "Fracture in Wire Drawing," M.S. Thesis, M.I.T., Sept. 1965.

8 Backofen, W.A., "Fracture of Engineering Materials," American Society for Metals, 1964.

9 Hoffmanner, A.L., "Development of Workability Testing Techniques," Interim Engineering Progress Report Oct., 1968. MMP Project No. 120-7, Metallurgical Processing Branch, Manufacturing Tech. Div., Wright-Patterson Air Force Base, Ohio.

10 Avitzur, B., "Analysis of Center Bursting Defects in Drawing and Extrusion," J. of Eng. for Ind., Trans., ASME Series B, Vol. 90, No. 1, Feb. 1968, pp. 79-91.

11 Zimerman, Z., Darlington, H., and Kottcamp, E.H., Jr., "Selection of Operating Parameters to Prevent Central Bursting Defects During Cold Extrusion," Article in "Metal Forming Interpretation Between Theory and Practice," Plenum Press, N.Y. 1971, pp. 47-62.

12 Avitzur, B., "Metal Forming: Processes and Analysis," 1st Edition, McGraw-Hill Book Co., N.Y., 1968, 2nd revised edition, Krieger, Huntington, N.Y., 1979.

13 Avitzur, B., "Metal Forming: The Application of Limit Analysis," Marcel Dekker, Inc., New York, 1980.

14 Rouse, H., (ed.), "Advanced Mechanics of Fluids," John Wiley & Sons, Inc., New York, 1959.

15 Sokolnikoff, I.S.,"Mathematical Theory of Elasticity," 2nd ed., McGraw-Hill, New York, 1956, pp. 117-184.

APPENDIX

Determination of the Radial Coordinate r_{fs}^* of the Surface of Discontinuity Γ_{ls}.

The principle of volume constancy requires that the normal component of velocity across the surface of discontinuity Γ_{ls} must remain continuous. The radial distance r_{fs}^* of this surface Γ_{ls} from the center of the toroidal coordinate system can, therefore, be found from the principle of volume constancy.

As shown in Fig. 12, each plane AA', normal to the surface Γ_{ls}, makes an angle ψ with the radial direction. Thus, the velocity continuity of the normal component acress Γ_{ls} surface dictates

$$-(\dot{U}_{rs})_{r=r_{fs}^*} \cdot \cos\psi = v_{fs} \cos(\psi-\theta) \tag{66}$$

where ψ is defined by Eq. (46) as

$$\psi = \tan^{-1}\left(\frac{1}{r_{fs}^*}\frac{dr_{fs}^*}{d\theta}\right) \tag{46}$$

Substituting $(\dot{U}_{rs})_{r=r_{fs}^*}$ of Eq. (5) and Eq. (46) into Eq. (66) leads to

$$(\tan\theta)\frac{dr_{fs}^*}{d\theta} + r_{fs}^* - \frac{v_{os}}{v_{fs}} \cdot \frac{r_{os}(r_{os}\sin\theta + e)}{(r_{fs}^* \sin\theta + e)} = 0 \tag{67}$$

Eq. (67) is a first-order differential equation with the boundary condition

$$(r_{fs}^*)_{\theta=\alpha} = \frac{R_f - e}{\sin\alpha} \tag{68}$$

After lengthy manipulations, the solution of Eq. (67) is obtained as

$$r_{fs}^*(\theta,e,\varepsilon) = \frac{-e}{\sin\theta} + \frac{R_o}{\sin\theta}\left\{\frac{v_{os}}{v_{fs}}\left[\left\langle\frac{\sin\theta}{\sin\alpha} + \frac{e}{R_o}\left(1 - \frac{\sin\theta}{\sin\alpha}\right)\right\rangle^2 - 1\right] + \left(\frac{R_f}{R_o}\right)^2\right\}^{1/2} \tag{10}$$

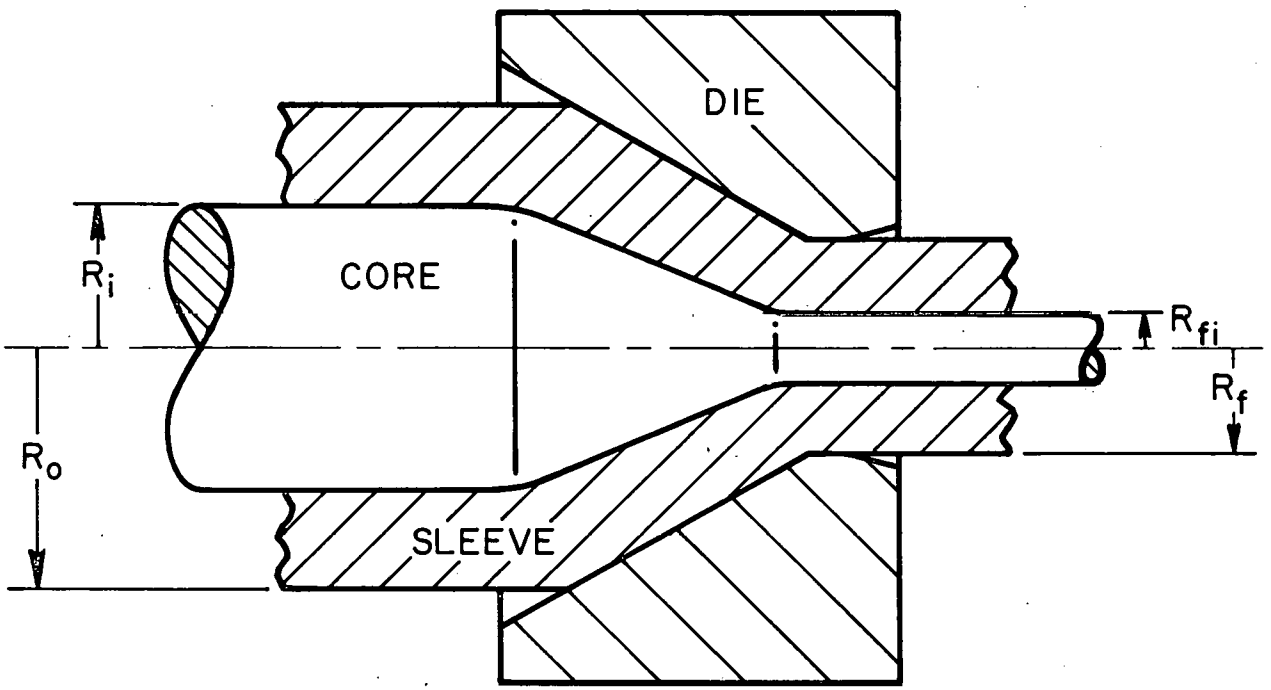

FIG.1 DIE, CORE AND SLEEVE.

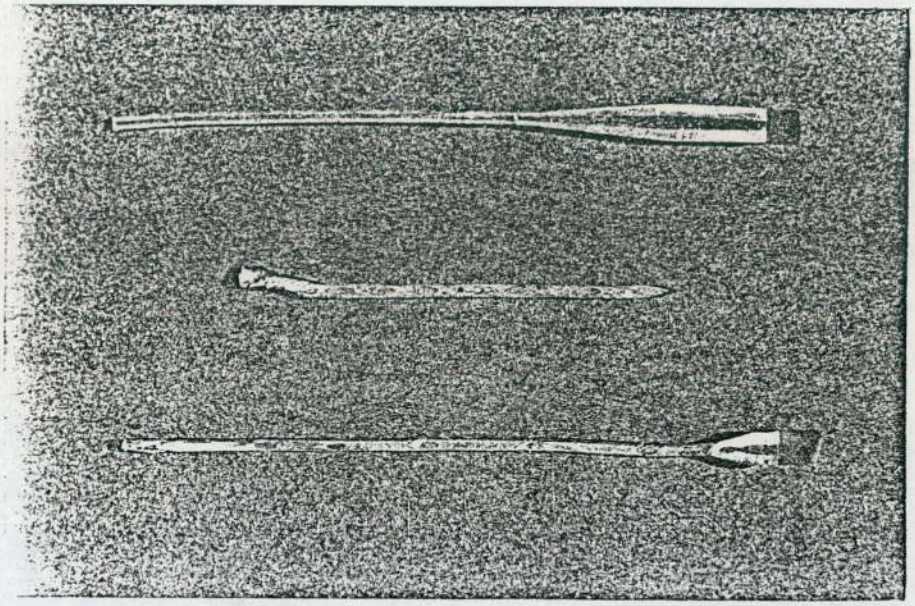

FIG.2a PROPORTIONAL FLOW AND CORE FRACTURE.

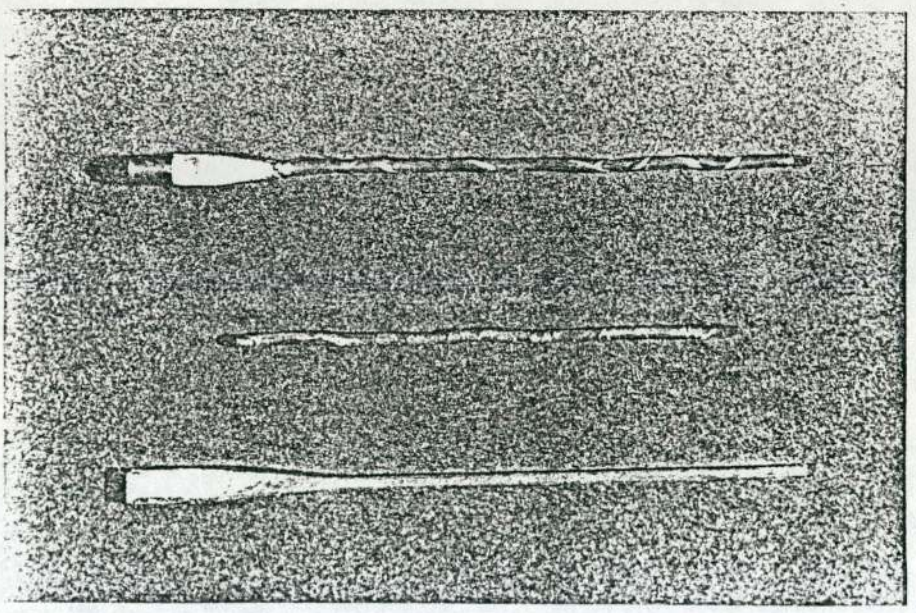

FIG.2b PROPORTIONAL FLOW AND SLEEVE FRACTURE.

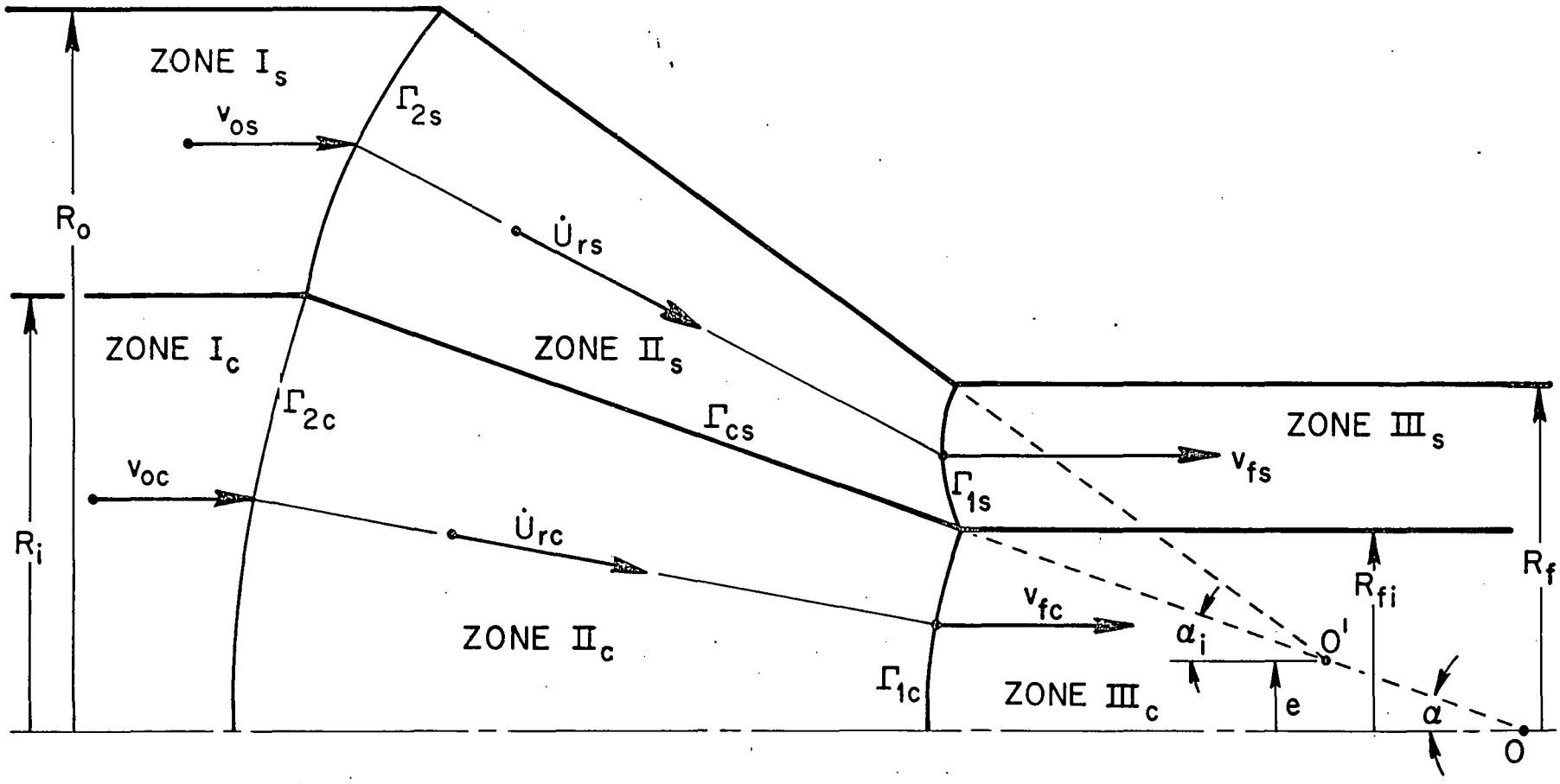

FIG.3 COMBINED FLOW IN CO-EXTRUSION.

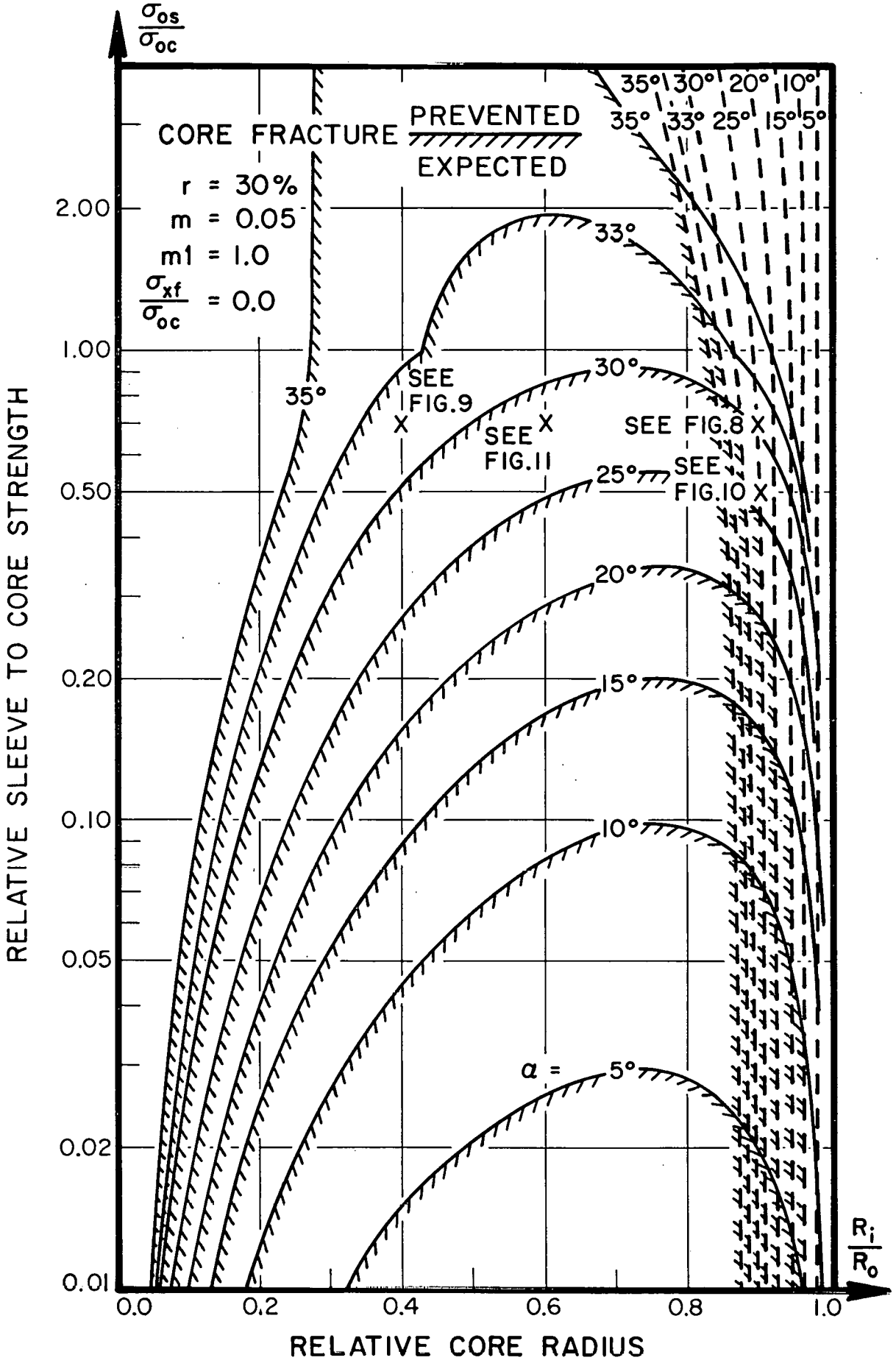

FIG.4a CRITERION FOR CORE FRACTURE IN EXTRUSION. (σ_{os}/σ_{oc} VS. R_i/R_o WITH CHANGING α)

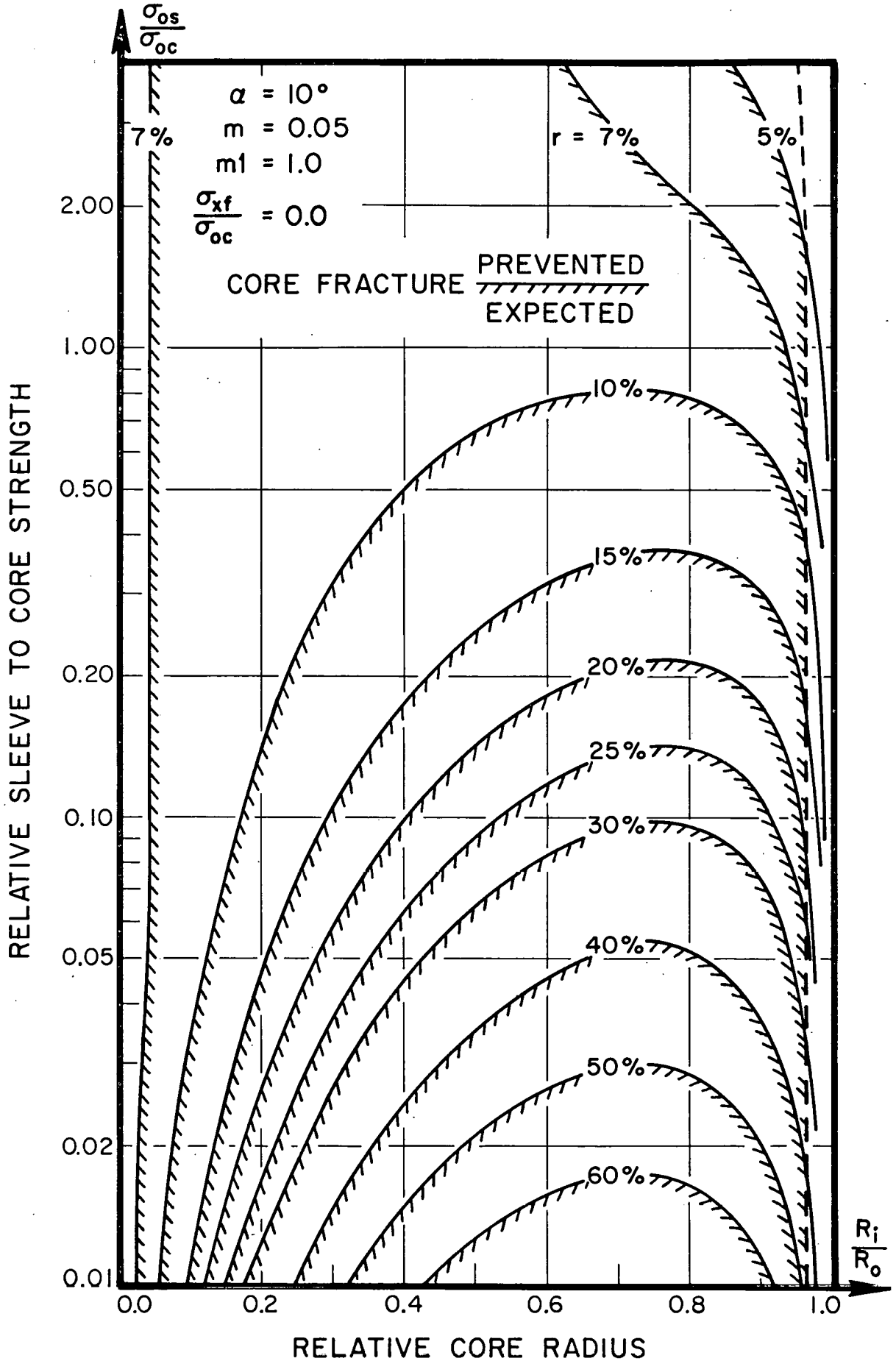

FIG. 4b CRITERION FOR CORE FRACTURE IN EXTRUSION. (σ_{os}/σ_{oc} VS. R_i/R_o WITH CHANGING r %)

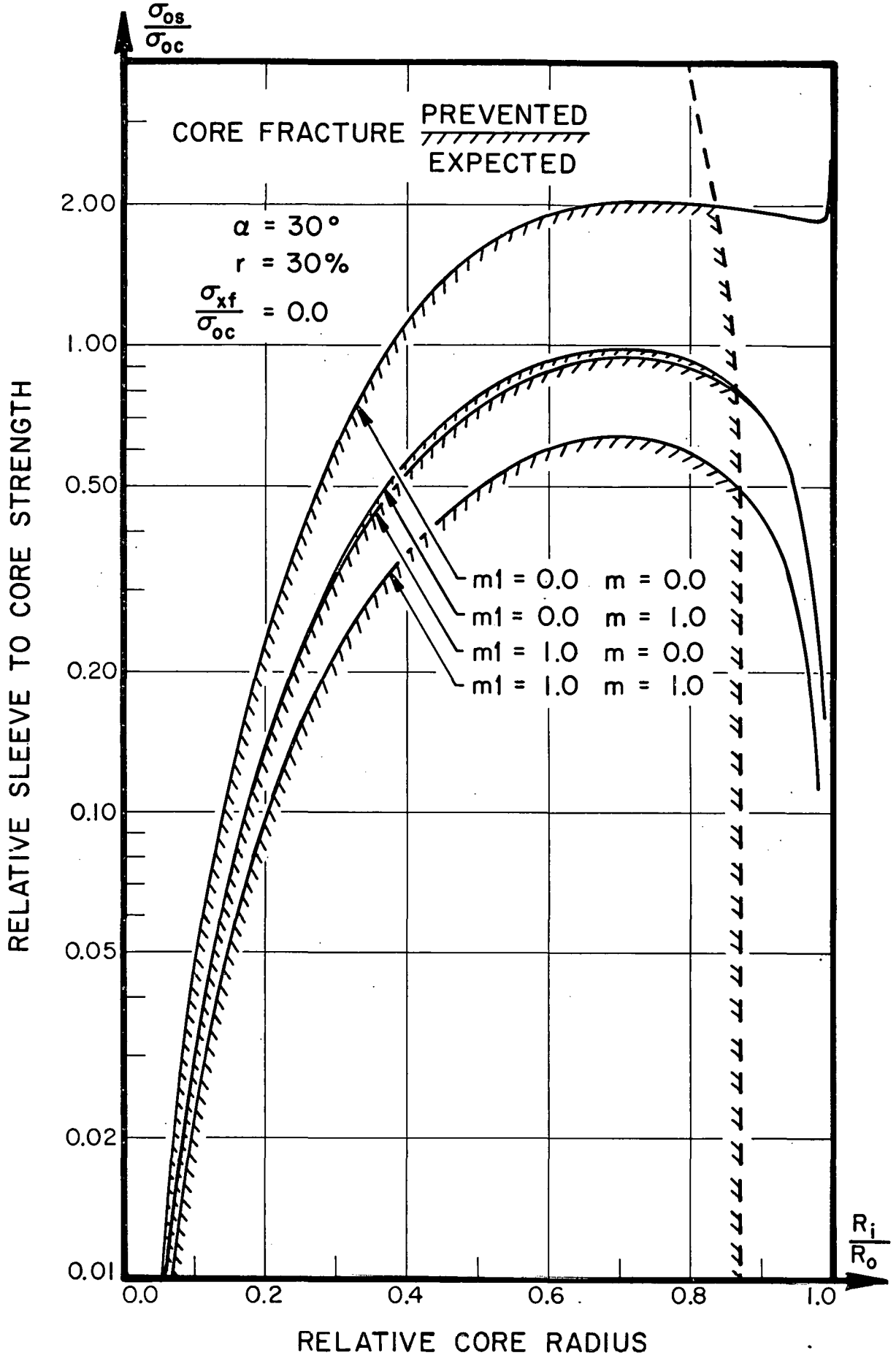

FIG. 4c CRITERION FOR CORE FRACTURE IN EXTRUSION. (σ_{os}/σ_{oc} VS. R_i/R_o WITH CHANGING m1 AND m)

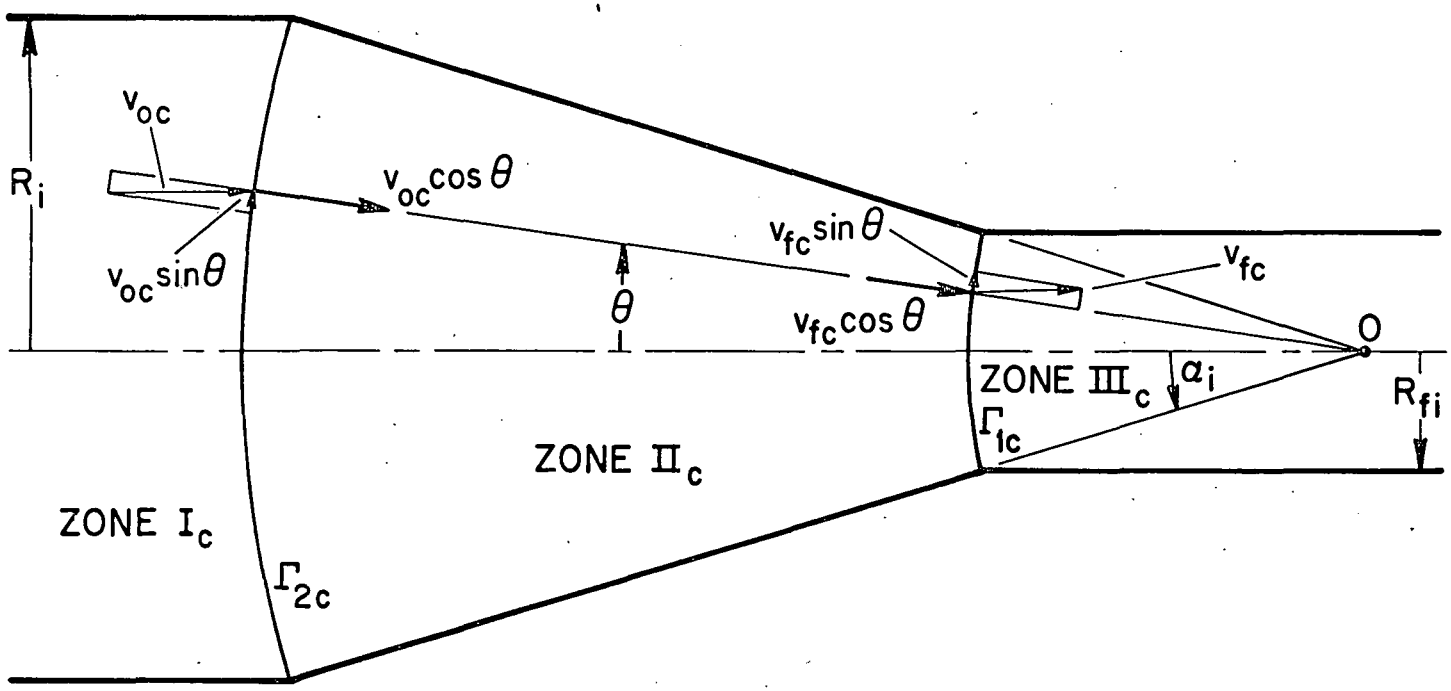

FIG.5 THE SPHERICAL VELOCITY FIELD FOR THE CORE.

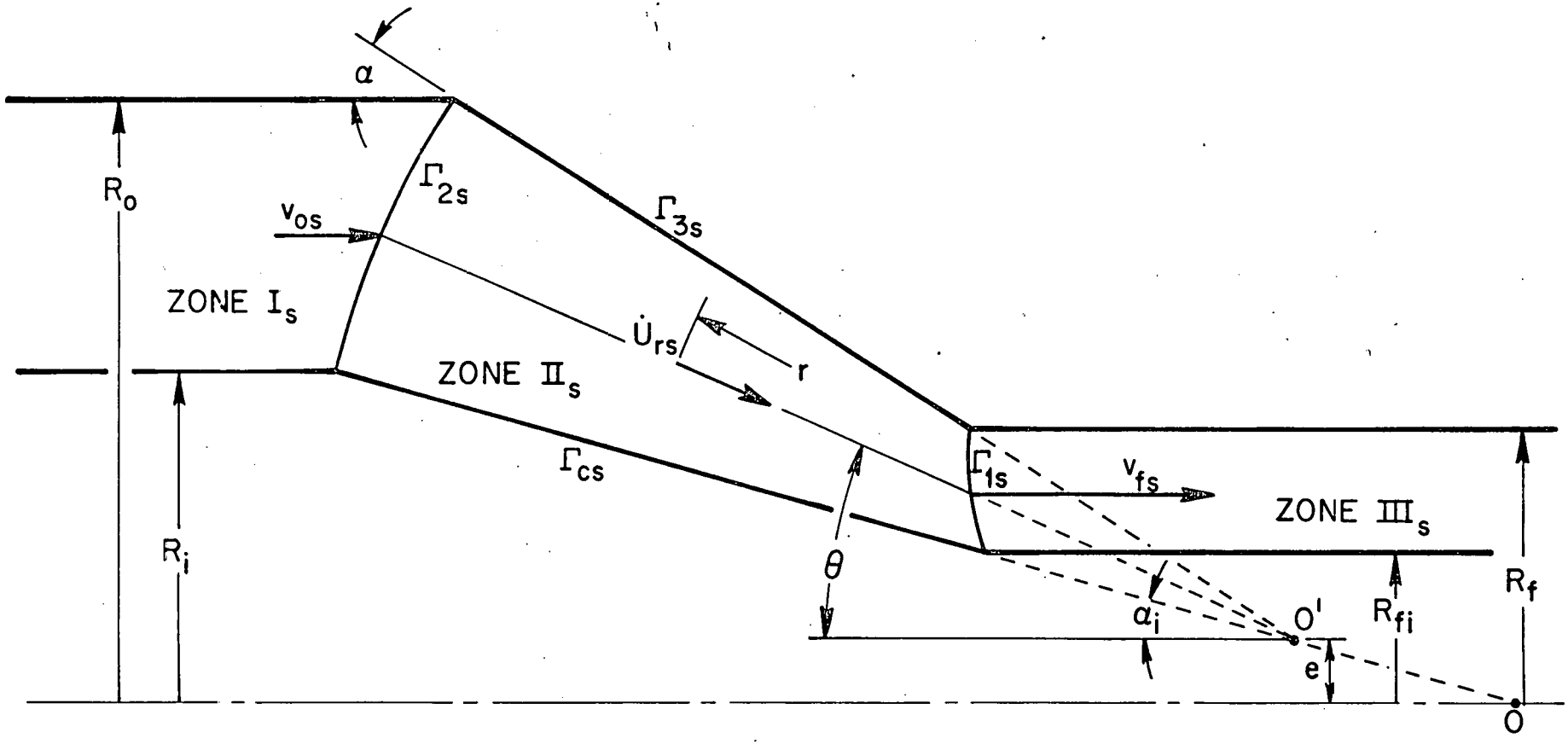

FIG.6 THE TOROIDAL VELOCITY FIELD FOR THE SLEEVE.

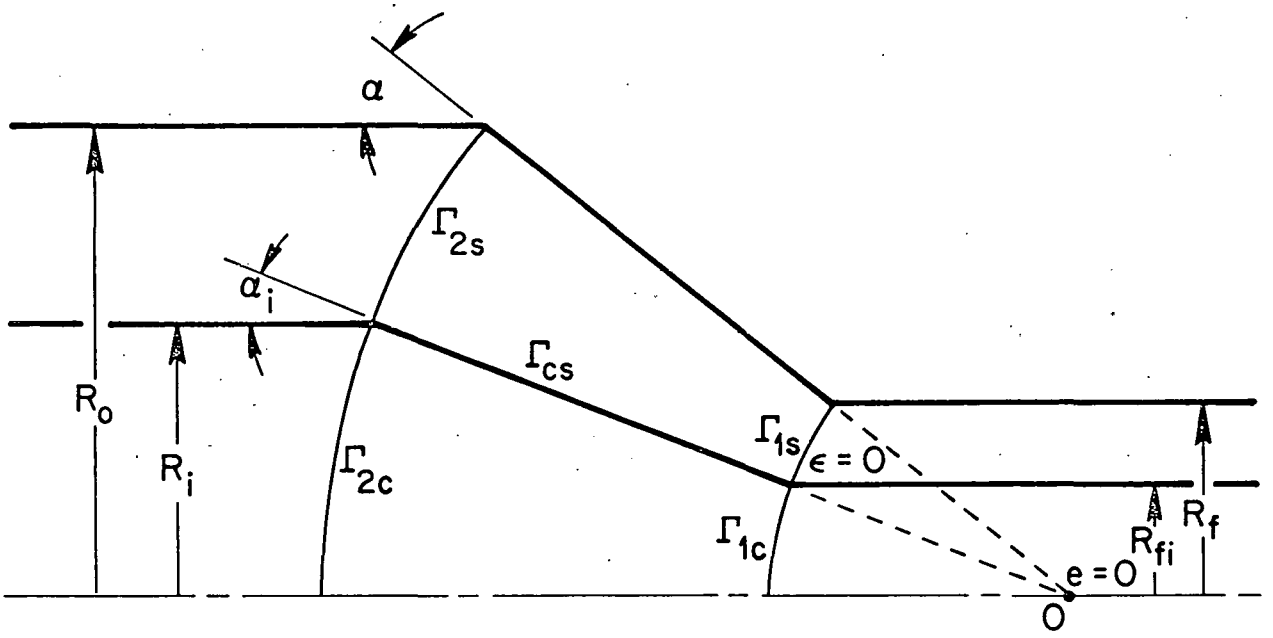

(a) PROPORTIONAL FLOW OF THE SLEEVE WITH e = 0.

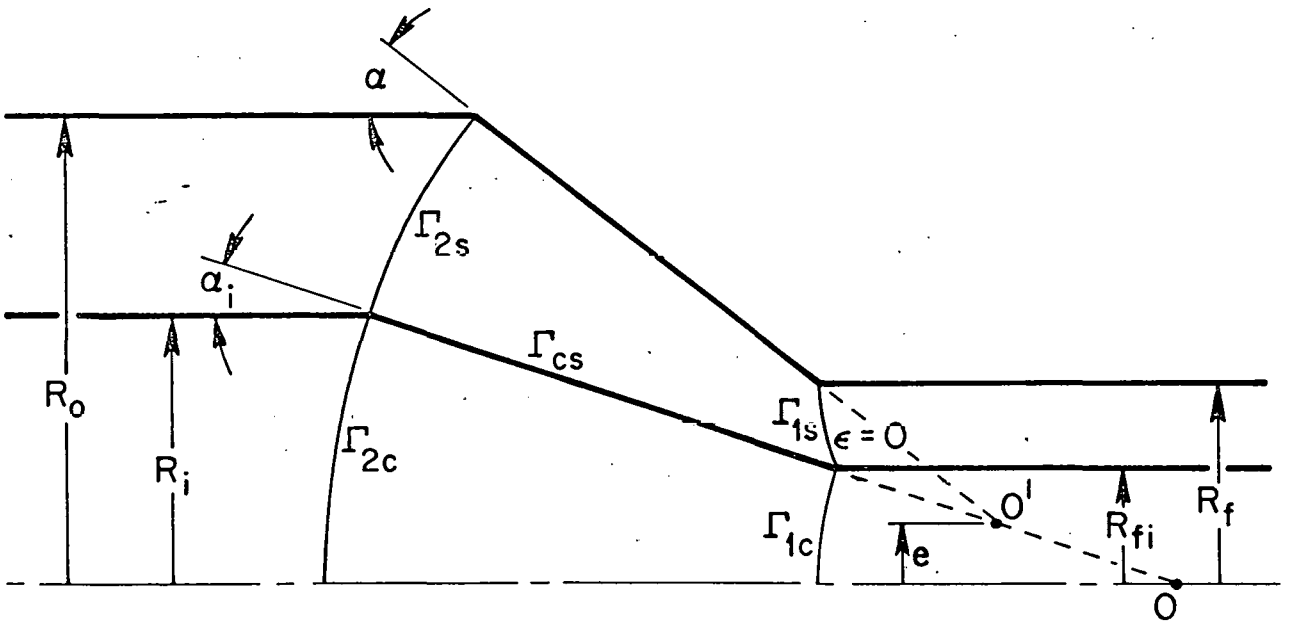

(b) PROPORTIONAL FLOW OF THE SLEEVE WITH e ≠ 0.

FIG.7 DETAIL VARIATIONS IN TOROIDAL VELOCITY FIELD.

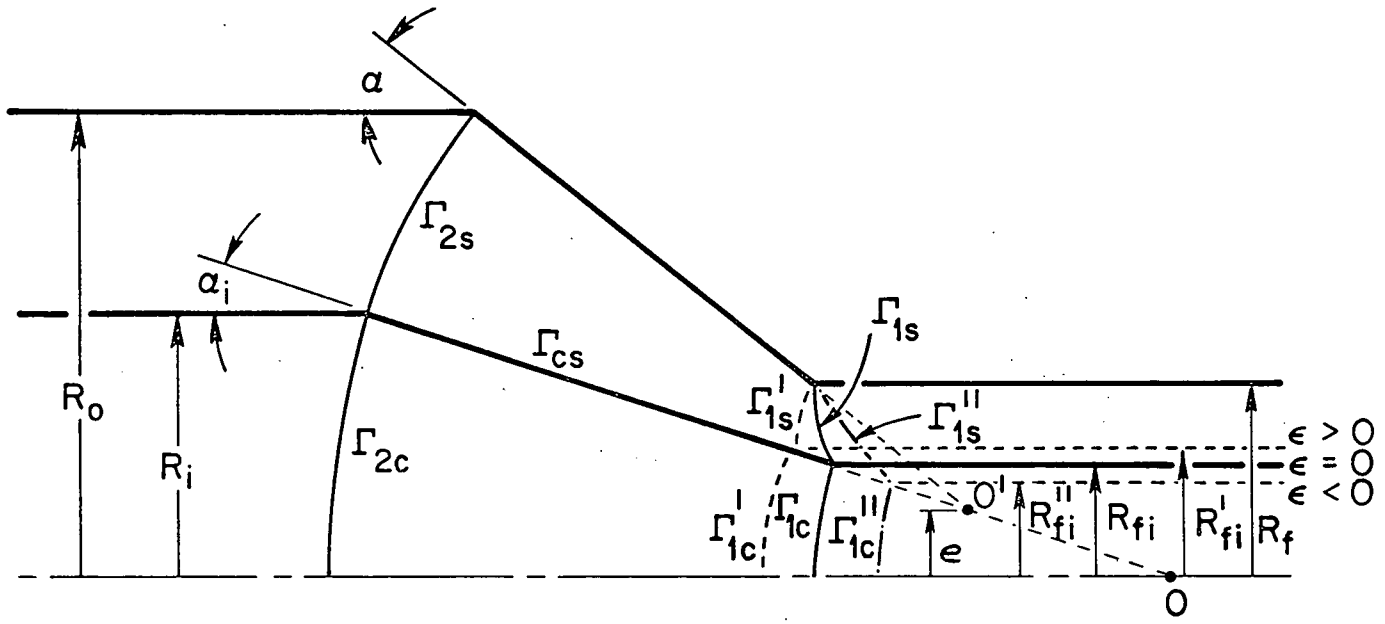

(c) THE EFFECT OF ϵ ON SLEEVE THINNING AND THICKENING.

FIG.7 DETAIL VARIATIONS IN TOROIDAL VELOCITY FIELD.

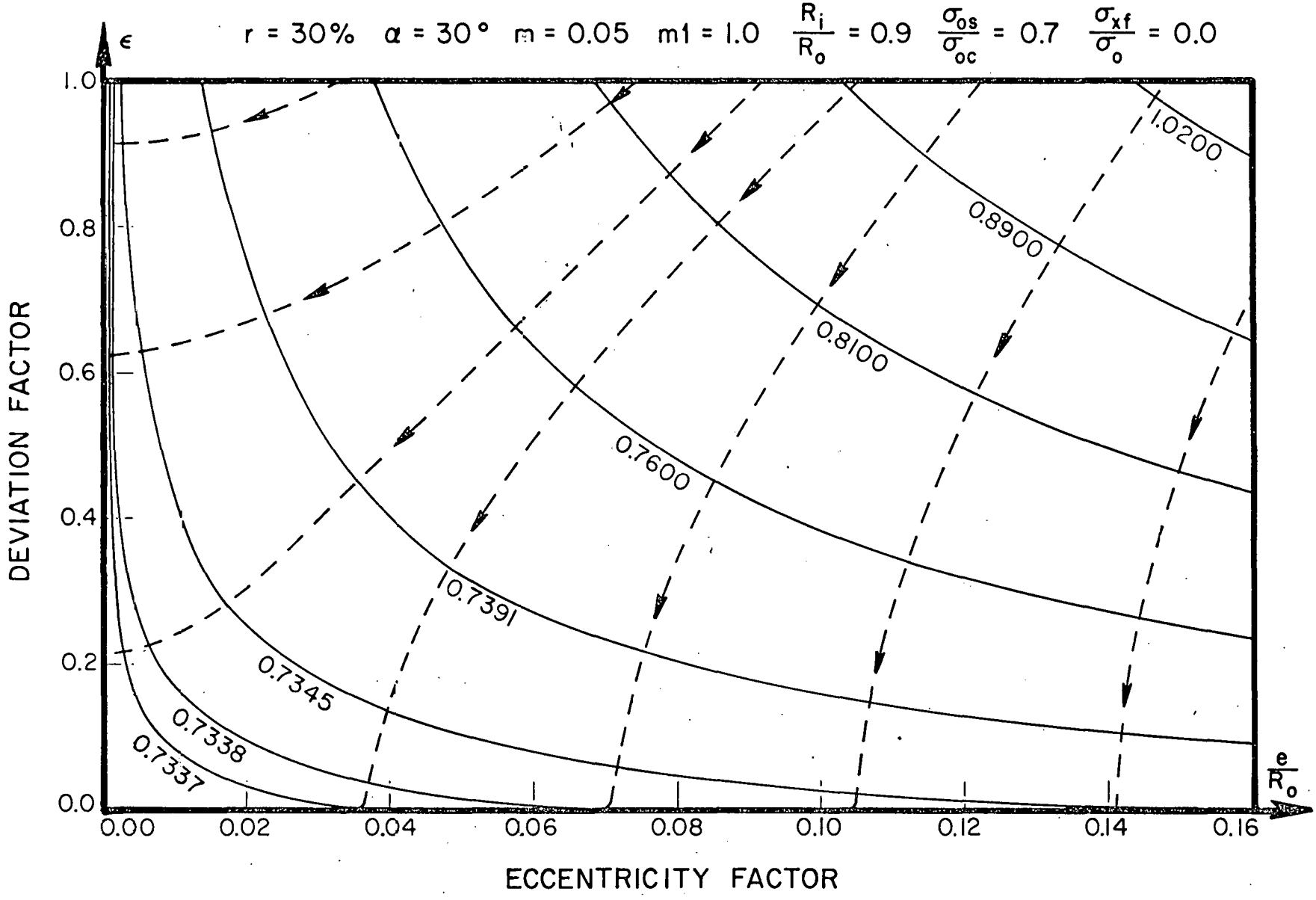

FIG.8 $\dot{J}^*$ CONTOUR FOR PROPORTIONAL FLOW WITH GLOBAL MINIMUM AT ORIGIN .

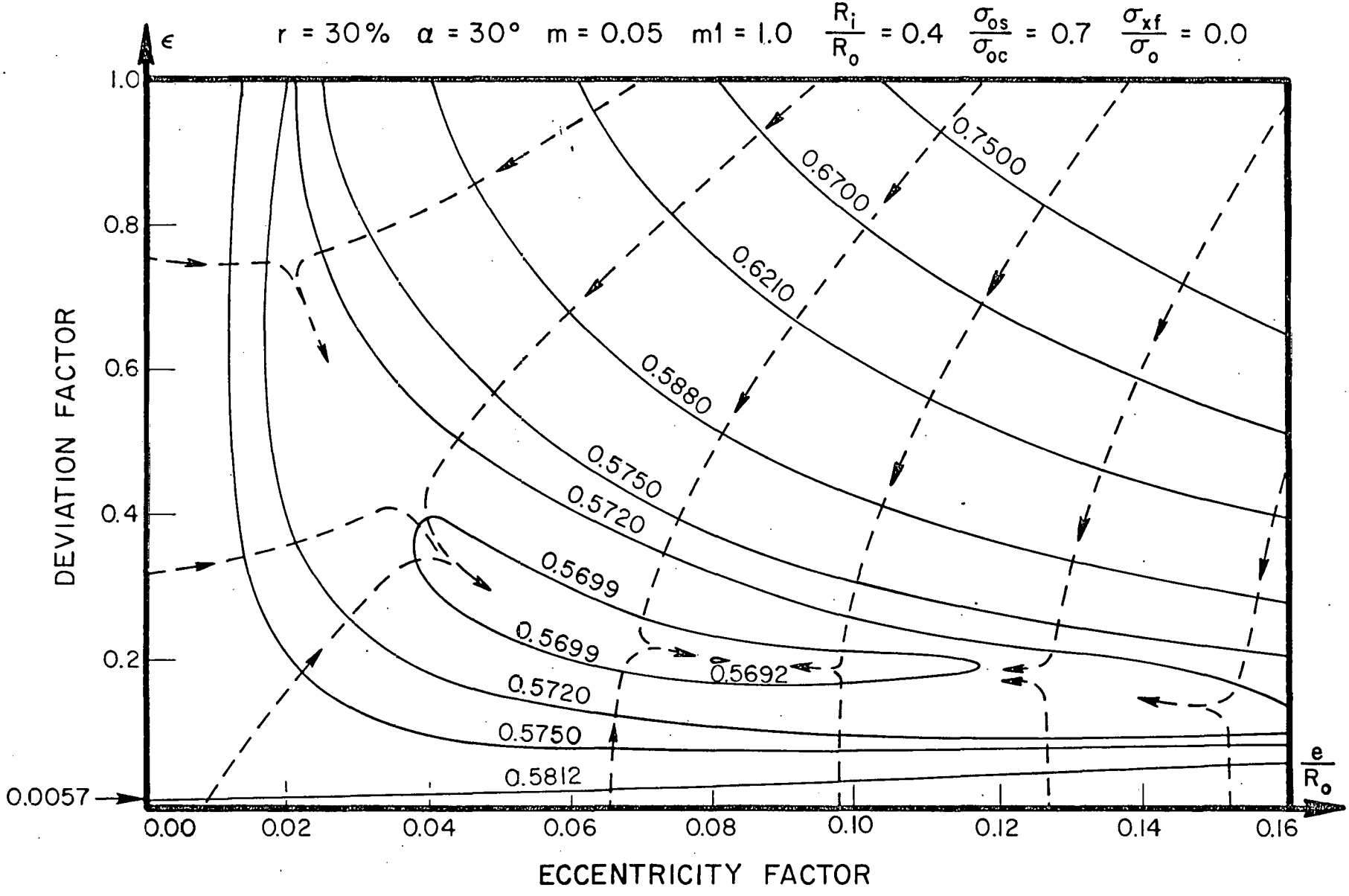

FIG.9a j^* CONTOUR FOR PROPORTIONAL FLOW.
(WITH LOCAL MINIMUM AT ORIGIN)

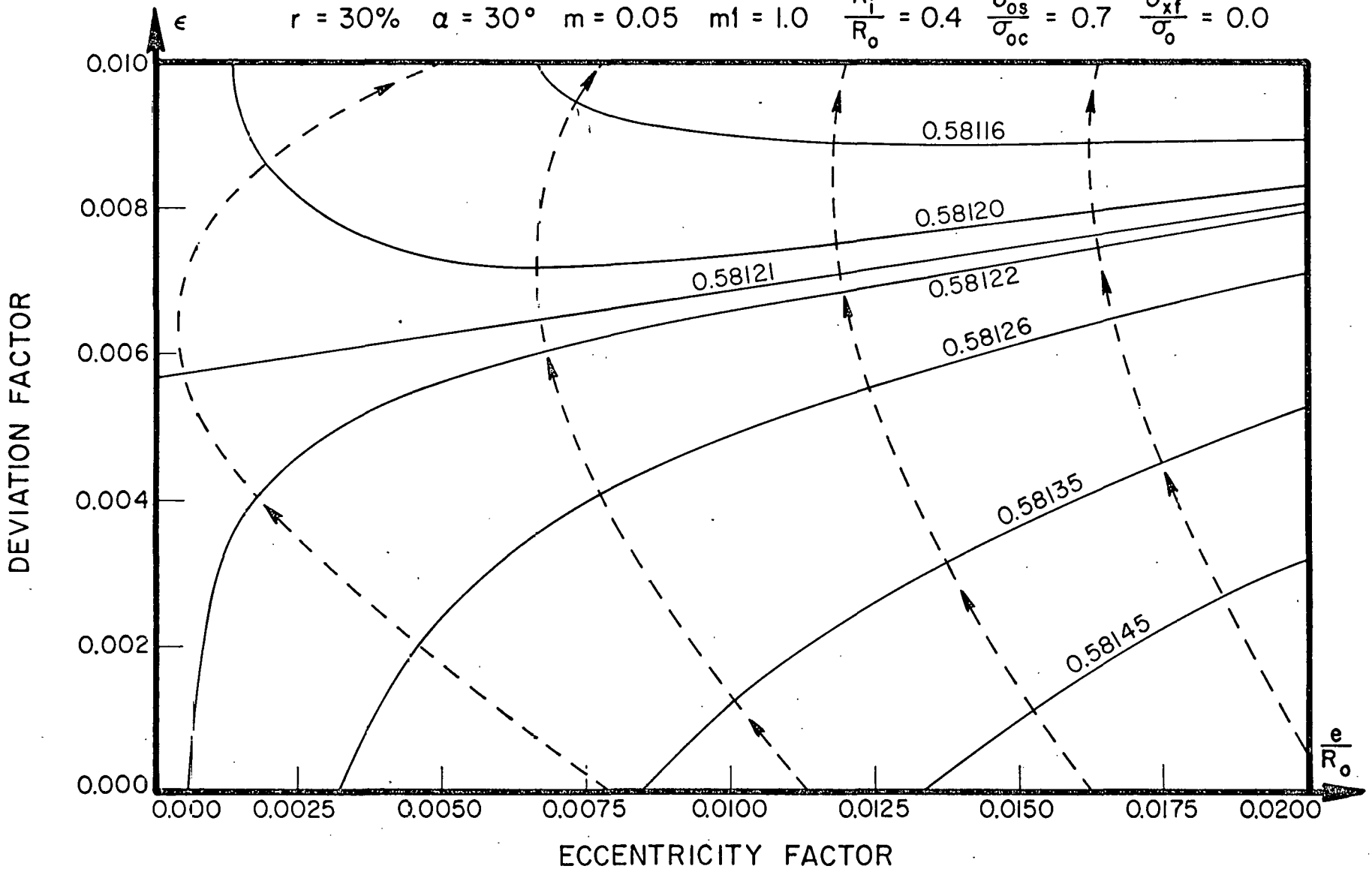

FIG.9b j^* CONTOUR FOR PROPORTIONAL FLOW.
(ENLARGED PORTION OF FIG.9a)

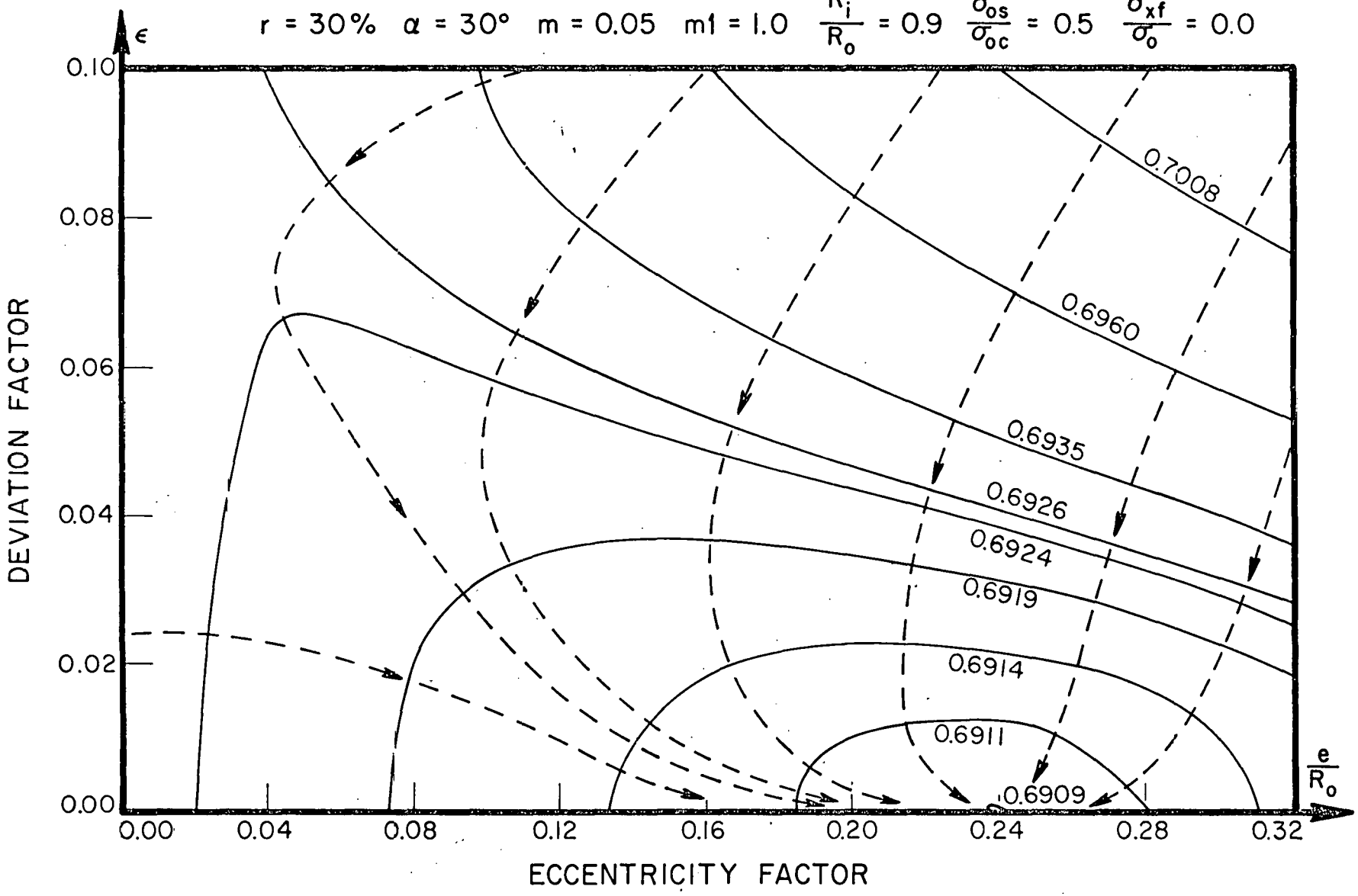

FIG.10 j^* CONTOUR FOR PROPORTIONAL FLOW WITH MINIMUM ON e/R_o AXIS.

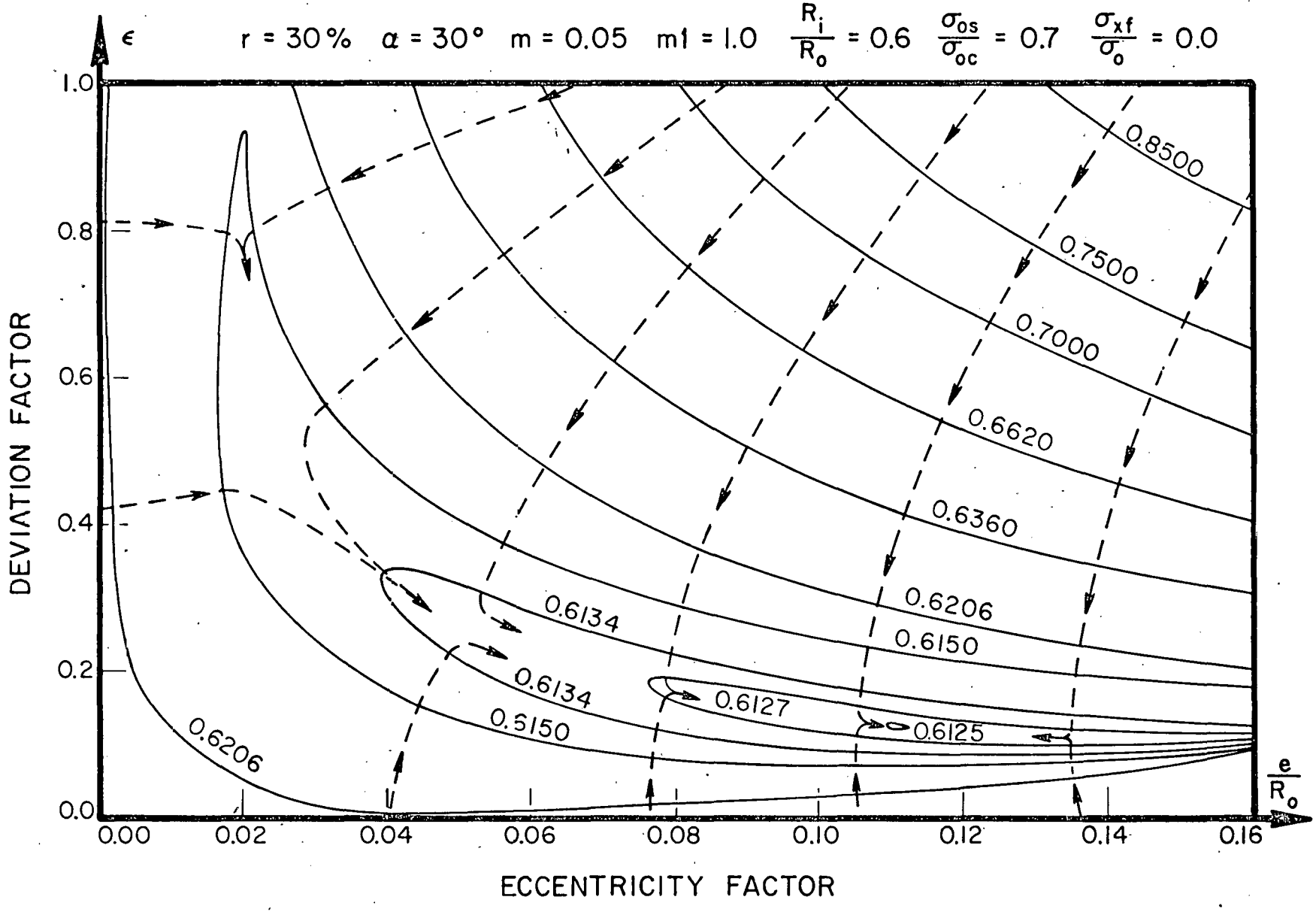

FIG. 11 J^* CONTOUR FOR CORE FRACTURE.

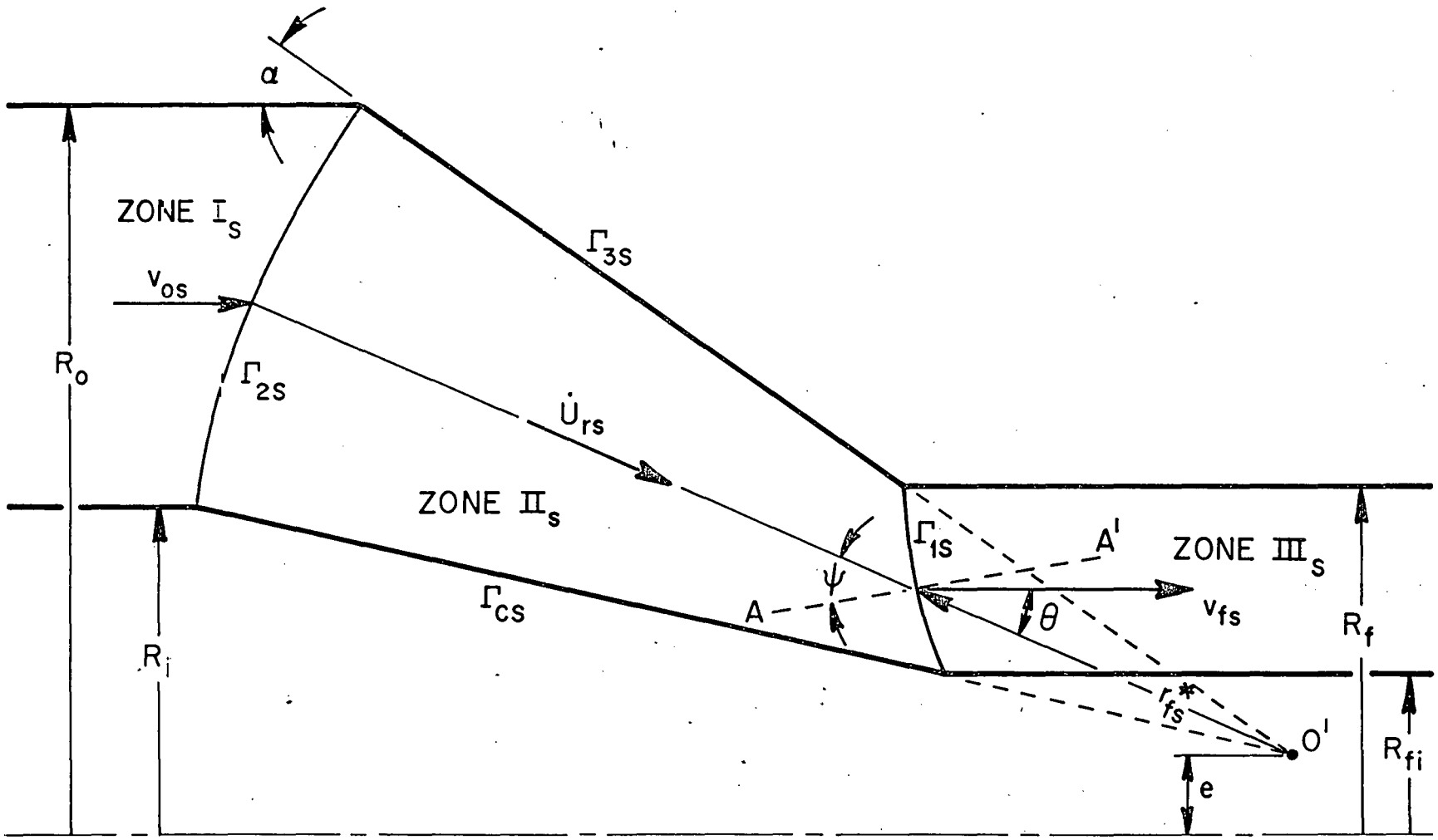

FIG.12 DETERMINATION OF THE SURFACE OF VELOCITY DISCONTINUITY AT THE EXIT SIDE OF THE SLEEVE.